ACS ES&T Air

pubs.acs.org/estair

Article

Effect of the Alkoxy Radical Chemistry on the Ozone Formation from Anthropogenic Organic Compounds Investigated in Chamber Experiments

Michelle Färber, Hendrik Fuchs,* Birger Bohn, Philip T. M. Carlsson, Georgios I. Gkatzelis, Andrea C. Marcillo Lara, Franz Rohrer, Luc Vereecken, Sergej Wedel, Andreas Wahner, and Anna Novelli*

Cite This: *ACS EST Air* 2024, 1, 1096−1111

Read Online

ACCESS | Metrics & More | Article Recommendations | Supporting Information

ABSTRACT: The photooxidation of five anthropogenic volatile organic compounds (propane, propene, isopentane, *n*-hexane, *trans*-2-hexene) at different levels of nitric oxide (NO) was investigated in the atmospheric simulation chamber SAPHIR, Forschungszentrum Jülich. Measured time series of trace gases and radical concentrations are compared to zero-dimensional box model calculations, based on the Master Chemical Mechanism (agreement within 30%) and complemented by state-of-the-art structure−activity relationships (SAR). Including RO_2 isomerization reactions from SAR, validated with theoretical calculations, improves particularly the model−measurement agreement by ∼20% for *n*-hexane. The photooxidation of the chosen compounds generates different types of peroxy radicals (RO_2) which produce HO_2 after one or multiple RO_2+NO reaction steps, depending on the formed alkoxy radical (RO). Measurements show that the HO_2/RO_2 ratio is up to ∼40% lower and the number of odd oxygen (O_x = O_3+NO_2) formed per OH+VOC reaction ($P(O_x)_{VOC}$) is up to ∼30% higher if RO regenerates RO_2 instead of forming HO_2 directly. Though, the formation of organic nitrates nearly completely compensates for the ozone production from the second NO reaction step for nitrate yields higher than 20%. Measured and modelled HO_2/RO_2 ratios agree well as does $P(O_x)_{VOC}$, derived from measured/modelled radical concentrations and calculated from measured O_x.

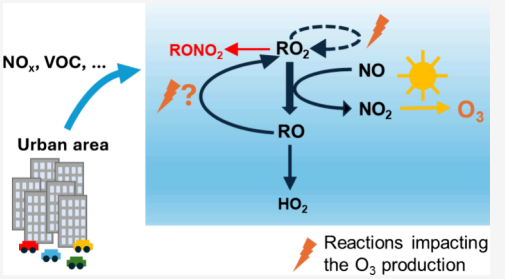

KEYWORDS: *Ozone production, Radical measurement, Anthropogenic VOCs, Master Chemical Mechanism, SAR, Alkoxy chemistry*

1. INTRODUCTION

Ozone pollution remains a health issue affecting millions of people residing in urban areas in Europe and worldwide.[1,2] In the troposphere, ozone (O_3) is produced by the photolysis of nitrogen dioxide (NO_2) subsequent to the reaction of hydroperoxy (HO_2) and organic peroxy (RO_2) radicals with nitric oxide (NO).[3] Although there has been a strong, continuous reduction of ozone precursors in urban emissions,[4−7] including volatile organic compounds (VOCs) and nitrogen oxides (NO_x = NO + NO_2) in the past decades, the decline in ozone levels has slowed in the summer in megacities,[8−10] highlighting the incomplete understanding of ozone production in urban environments.

HO_2 and/or RO_2 radicals are intermediates formed in the atmospheric oxidation of volatile organic compounds. In urban environments, the reaction with NO remains currently their dominant chemical loss as NO mixing ratios are still up to a few ppbv especially during the morning traffic rush hour.[11,12] Field campaigns, performed in urban and remote environments where either only HO_2 radicals[13,14] or both, HO_2 and RO_2, radicals were measured,[15−20] have shown large discrepancies between measured and modelled radical concentrations. Deviations are highest for NO mixing ratios larger than 1 ppbv when measured radical concentrations are also underestimated by model calculations. In most of these studies, the measured HO_2 and RO_2 radical concentrations were used to calculate the instantaneous odd oxygen (O_x = O_3 + NO_2) production, showing large discrepancies with model results. The O_x production rate calculated from radical concentrations was for example up to a factor of 10 higher than derived from model calculations in London[16] and of 100 in Beijing.[15] As the Master Chemical Mechanism[21,22] (MCM; www.mcm.york.ac.uk) and the Regional Atmospheric Chemical Mechanism[23] (RACM) are used in chemical transport models to predict regional ozone pollution, the large model−measurement differences observed

Received: March 19, 2024
Revised: July 17, 2024
Accepted: July 17, 2024
Published: August 2, 2024

Table 1. Instrumentation for Radical and Trace-Gas Measurements, Available during the Presented Experiments in SAPHIR

Species	Technique	Time resolution	1 σ precision	1 σ accuracy
OH	DOAS	431 s	7.3×10^5 cm^{-3}	6.5%
	LIF	45 s	2.8×10^5 cm^{-3}	18%
HO_2	LIF	45 s	7.7×10^6 cm^{-3}	18%
RO_2	LIF	45 s	7.2×10^6 cm^{-3}	18%
NO	Chemiluminescence	98 s	3 pptv	5%
NO_2	Chemiluminescence	98 s	70 pptv	5%
O_3	UV absorption	60 s	90 ppbv	5%
VOCs[a]	GC-FID	42 min	40 pptv	5%
trans-2-hexene	PTR-TOF-MS	30 s	15 pptv	10%
CH_3CHO, Acetone	PTR-TOF-MS	30 s	60 pptv	20%
HCHO	PICARRO	120 s	120 pptv	10%
k_{OH}	Laser photolysis + LIF	142 s	0.06 s^{-1}	10%
j values	Spectroradiometry	30 s	4.8×10^{-8} s^{-1}[b]	10%

[a]Including propene, isopentane, and *n*-hexane. [b]Derived from j_{NO_2} data.

in different cities indicate a potential gap in the understanding of the ozone production chemistry.

Several hypotheses to explain the observed discrepancies were proposed in the different studies. Poor mixing and therefore segregation of NO and radicals was pointed out as a possible reason,[24] although instrument inlets were located in close proximity in most campaigns to avoid such complications.[15,17] Artifacts in the measurements could also be responsible for the observed differences. Radical measurements were performed by different groups, but they all applied the same detection method (laser-induced fluorescence, LIF). Peroxy radicals, HO_2 and RO_2, were detected using their chemical conversion to OH in the reactions with NO, so that the detection of HO_2 could have been biased by the concurrent conversion of RO_2.[25,26] Most of the recent studies were performed using instruments, in which such effects are minimized by using a reduced HO_2 conversion efficiency in the detection cell. In previous studies,[13] instruments used a quantitative conversion of HO_2 to OH in the detection cell, which in turn facilitated the additional conversion of RO_2 radicals. This makes the comparison of measurements and model results challenging.[27] The larger-than-modelled HO_2 radical concentration, observed in field studies, was often consistent with the required OH production rate from the reaction of HO_2 with NO to reproduce the observed OH radical concentrations,[19,28] making it unlikely that the high measured HO_2 radical concentrations were due to measurement artifacts.

Several potential mechanisms were tested in the evaluation of field campaigns to improve the model−measurement agreement between HO_2 and RO_2 radical concentrations:

- Additional radical sources were introduced in the model, e.g., from the photolysis of nitryl chloride ($ClNO_2$) or chlorine compounds.[17,19]
- The rate coefficients of the RO_2 and NO reactions were decreased by up to a factor of 5.[18,20]
- The conversion efficiency of RO_2 to HO_2 radicals was inhibited in the model by introducing RO_2 radicals undergoing multiple reactions with NO before an HO_2 radical is formed.[15,16]

In this work, the last hypothesis was investigated in 11 photochemistry experiments in the large outdoor atmospheric simulation chamber SAPHIR. Experiments explored the chemical degradation of a series of alkanes (propane, isopentane, *n*-hexane) and alkenes (propene, *trans*-2-hexene) and the concurrent ozone production at different NO levels between 0.1 ppbv and 6 ppbv. The chosen species are representative for VOCs abundant in urban areas[16,29−31] as well as for the different chemistry of the alkoxy (RO) radicals formed after the reaction of the primarily formed RO_2 radical with NO.[32,33] Measured concentrations are compared to results of zero-dimensional box model calculations using the MCM. Finally, calculations of the number of O_x molecules formed per OH + VOC reaction from either measured radical concentrations or the measured O_x concentration are compared.

2. METHODOLOGY

2.1. The Atmospheric Simulation Chamber SAPHIR. The experiments in this study were conducted in the outdoor atmospheric simulation chamber SAPHIR at the Forschungszentrum Jülich, Germany. The chemically inert double-wall Teflon (FEP) film has a high transmittance of the entire spectrum of the solar radiation, allowing the simulation of atmospheric processes under realistic tropospheric conditions. The cylindrically-shaped chamber has a total volume of 270 m^3 with a diameter of 5 m and a length of 18 m, resulting in a low surface-to-volume ratio of ∼1 m^{-1}. Two fans ensured that the same air composition is measured by all instruments. Ultra-pure synthetic air (79% N_2, 21% O_2, Linde, purity >99.9999%) is used. The chamber is operated with a small overpressure of about 25 Pa to prevent contamination from ambient air. The replenishment flow required to compensate for small leakages and the consumption of air by the instruments causes a dilution with a rate constant of $(5.0 \pm 0.8) \times 10^{-6}$ s^{-1}. The temperature inside the chamber is not controlled and is thus similar to ambient conditions. In the experiments in this work, temperatures of (304 ± 5) K were reached. The chamber is equipped with a shutter system. With open shutters, OH radicals are mainly produced by photolysis of nitrous acid (HONO), which is released from the chamber film with a rate that depends on sunlight intensity, humidity, and temperature.[34] Further details of the atmospheric simulation chamber SAPHIR can be found in previous publications.[34−37]

2.2. Instrumentation. An overview of the used instrumentation is shown in Table 1.

OH, HO_2, and RO_2 radicals were detected with a laser-induced fluorescence (LIF) instrument (RO_xLIF).[38,39] Air is pulled through a conically shaped nozzle into a low-pressure detection cell (∼4 hPa). Inside the detection cell, OH radicals are excited by a short laser pulse (wavelength = 308 nm, repetition rate = 8.5 kHz) and their fluorescence is detected.

https://doi.org/10.1021/acsestair.4c00064
ACS EST Air 2024, 1, 1096−1111

The corresponding photon count rate, which is directly proportional to the sampled OH radical concentration, is measured by a gated microchannel plate detector.[40−42]

In the experiments in this work, the OH detection cell was equipped with a chemical modulation reactor (CMR),[42] allowing for interference-free OH radical measurements. In the CMR, propane (Air Liquide, purity >99.95%, (5.0 ± 0.1)% mixture in N_2) acting as an OH scavenger is periodically injected. In all experiments performed in this work, the observed interference signal could be entirely attributed to the well-characterized interference caused by the production of OH from the photolysis of ozone by the excitation laser inside the measurement cell.[39] In a second detection cell, HO_2 is indirectly measured by its conversion to OH in the reaction with the injected NO, such that the sum of both (HO_x = OH + f·HO_2, f < 1 being dependent on the NO concentration in the detection cell) is detected.[25,39−41] The HO_2 radical concentration can be derived by subtracting the measured OH radical concentration. Interferences may appear in the HO_x measurement in the presence of specific RO_2 radicals, which rapidly form HO_2 following the RO_2 + NO reaction.[25] This RO_2 interference is minimized by working with low NO concentrations and did not play a role in the presented experiments. In a third detection system, the total RO_x (= OH + HO_2 + RO_2) radical concentration is measured. The RO_2 radical concentration can be determined by subtracting the measured OH and HO_2 radical concentrations. Air is introduced into a converter (∼25 hPa), where RO_2 radicals are first converted to HO_2 and then to OH in reactions with added NO. By also adding CO in excess, OH radicals, mainly formed from the reaction of HO_2 with NO, are converted back to HO_2 in the converter. The HO_2 radicals are then converted to OH in the reaction with injected pure NO in another low-pressure detection cell downstream of the converter, aiming for a complete conversion of HO_2 radicals to OH.[38] In the HO_x and RO_x detection cells, in which NO is added, a background signal that is equivalent to radical concentrations of (6.2 ± 0.5) × 10^7 cm^{-3} and (5.6 ± 2.6) × 10^7 cm^{-3}, respectively, was observed. The values were determined during calibrations of the RO_xLIF instrument performed with clean, humidified synthetic air. The mechanism behind the NO background has not yet been clarified.

OH radicals were also measured by differential optical absorption spectrometry (DOAS) in five experiments. The DOAS technique is an absolute measurement technique. Laser pulses at a wavelength of 308 nm produced from a picosecond dye laser system are coupled into the chamber and reflected more than 100 times along its longitudinal axis to achieve a 2 km long absorption path. The transmitted light is then analyzed by a high-resolution spectrometer to determine the absorption by the OH radicals. OH radical concentrations, measured by the LIF and the DOAS instruments, agree within 20% in the experiments in this work.

Cavity ring-down spectroscopy[43] (CRDS, Picarro) was used to detect formaldehyde (HCHO) and water vapor. Ozone was detected by UV absorption (Ansyco), and NO and NO_2 were detected by using chemiluminescence (EcoPhysics).

The OH reactivity (k_{OH}), equivalent to the inverse of the OH lifetime, was measured by a laser-photolysis pump-and-probe technique, using the LIF technique to detect the decay of artificially produced OH reacting with the OH reactants in the sampled air in a flow tube.[44,45]

Time series of propene and *trans*-2-hexene were measured by proton-transfer-reaction time-of-flight mass spectrometry (PTR-ToF-MS, Ionicon),[46,47] while isopentane and *n*-hexane were measured by gas chromatography combined with a flame-ionization detector (GC-FID).[48] The signals at the masses of injected VOCs were converted to concentrations by scaling them such that the corresponding increase in the OH reactivity matched the increase observed by the OH reactivity instrument at the point in time of the VOC injection. Calibrated time series of acetone and acetaldehyde (CH_3CHO) were measured by the PTR-ToF-MS instrument.

Photolysis frequencies such as of NO_2, HONO, O_3, CH_3CHO, and HCHO were derived from measurements of the total and diffuse spectral actinic flux densities using a spectroradiometer that is located on the top of a building next to the chamber.[49,50] Calculations take into account the transmittance of the chamber foil and local shading from the construction elements of the chamber.

2.3. Experimental Procedure. Eleven experiments were performed, with five anthropogenic VOCs (propane, propene, isopentane, *n*-hexane, and *trans*-2-hexene) at NO mixing ratios between 0.1 ppbv and ∼9 ppbv.

At the beginning of each experiment, the clean chamber air was humidified in the dark to reach a water vapor mixing ratio of about 1%. An OH reactivity up of 1.5 s^{-1} was observed after the humidification in the clean chamber caused by mainly unknown reactants, likely released by the chamber wall during the humidification (OH background reactivity).

In the experiments that aimed for NO mixing ratios lower than ∼0.4 ppbv, about 80 ppbv ozone was injected before the chamber's shutter was opened. To achieve NO mixing ratios larger than 1 ppbv in the chamber for the duration of the experiment, NO was continuously added into the sunlit chamber with a rate of up to 7 ppbv h^{-1}, reaching NO mixing ratios of up to 8.5 ppbv. In all experiments, the shutter system of the chamber was open for about an hour before the VOC was injected to quantify the small emissions from the chamber foil by observing their increase in concentration. Throughout most experiments, VOC was injected multiple times. The following anthropogenic VOCs were tested: propane (Air Liquide, 5% in N_2, purity 99.5%), propene (Air Liquide, 1% in N_2, purity 99.96%), isopentane (Fluka, purity 99%), *n*-hexane (Sigma-Aldrich, purity >99%), and *trans*-2-hexene (Sigma-Aldrich, purity 97%).

For the experiments presented in this study, the wall emission rates of released compounds were estimated to be for nitrous acid: ∼(0.6 ± 0.3) $ppbvh^{-1}$, for formaldehyde: ∼(0.42 ± 0.20) $ppbvh^{-1}$, for acetaldehyde: ∼(0.27 ± 0.11) $ppbvh^{-1}$, and for acetone: ∼(0.09 ± 0.04) $ppbvh^{-1}$. In the experiments performed in this work, an additional chamber source of NO_x was observed, which might be related to the release of nitrates from the chamber wall in the presence of sunlight. The wall emission rate of NO was estimated to be (0.47 ± 0.44) $ppbvh^{-1}$.

In the experiments with NO > 1 ppbv, HO_2 and RO_2 radicals had a short chemical lifetime of less than 2 s, so that their concentrations were comparable to the NO background, observed in the HO_x and RO_x detection cells (Section 2.2). At high NO conditions, the signal-to-background ratios were less than two for the HO_x and RO_x measurement. In comparison, an average signal-to-background ratio of 7 and 12 was achieved in the HO_x and RO_x measurement, respectively, in the experiments at NO < 1 ppbv. The low signal-to-background ratio resulted in large uncertainties in the measured HO_2 and RO_2 radical concentrations at high NO. Therefore, the radical data for these

https://doi.org/10.1021/acsestair.4c00064
ACS EST Air 2024, 1, 1096−1111

experiments are not used in the analysis. An overview of the experimental conditions is given in Table 2.

Table 2. Conditions of the Experiments Presented in This Work[a]

VOC	Experiment	[NO] (ppbv)	[OH] (10^6 cm^{-3})	[VOC] (ppbv)
NO < 1 ppbv				
propane[b]	13th of May 07th of June	0.04–0.7	(2.2 ± 1.1)	410–580
propene	09th of June	0.04–0.18	1.9 ± 0.6	11–17
isopentane[b]	11th of June 21st of June	0.1–0.9	(1.8 ± 1.3)	105–145
n-hexane	19th of May	0.1–0.3	1.9 ± 0.7	55–130
trans-2-hexene	24th of May	0.07–0.6	2.2 ± 0.9	≤10.5
NO > 1 ppbv				
propane	18th of May	2.1–6.2	3.3 ± 1.7	245–364
propene	23rd of June	1.3–10.7	3.7 ± 1.4	2–28
isopentane	16th of June	2.1–9.8	2.6 ± 0.6	145–191
n-hexane	22nd of May	2.0–6.1	1.8 ± 0.6	58–98

[a]The values correspond to mean values ([OH]) or the range of values ([NO], [VOC]) during the photooxidation part of the experiments. Values are given for experiments with NO < 1 ppbv and with NO > 1 ppbv. [b]Two experiments considered.

2.4. Model Calculations. Measured concentrations of OH, HO_2, and RO_2 radicals, as well as of trace gases (NO, NO_2, O_3, HCHO, CH_3CHO, and acetone), and of the OH reactivity are compared to results from zero-dimensional box model calculations, based on the chemical mechanistic information of the Master Chemical Mechanism v3.3.1 (MCM; www.mcm.york.ac.uk).[21,22] Temperature, pressure, and photolysis frequencies are constrained to the measurements, and the dilution of the chamber air is taken into account as a first-order loss process (Section 2.1). Parametrizations of the chamber-related emissions of NO, HONO, HCHO, CH_3CHO, and acetone in the sunlit chamber, which depend on radiation, relative humidity, and temperature,[34,51] (Section 2.3) are included in the model. For each experiment, the production rates are scaled to match the observed trace gas concentrations in the sunlit chamber before the injection of the VOC of interest (Section 2.3). Since HONO was not measured in the experiments, its chamber source in the model was adjusted by matching the observed increase in OH radical concentration, as HONO photolysis was the only OH source in the clean chamber besides ozone photolysis in most of the experiments with low NO mixing ratios. The background OH reactivity, observed in the dark before the reactants were added, is described in the model by an OH reactant that behaves like CO. In the sunlit chamber, NO, NO_2, and to a small extent small oxygenated compounds add to the OH reactivity. The background OH reactivity is assumed to be constant throughout the experiment. Injections of O_3, NO, and VOC into the chamber are implemented in the model as an active source during the injection period, whose strength is adjusted to match the measured increase of their concentrations.

For all VOCs, an extended chemical mechanism (called MCM+SAR, MCM+SAR+THEO for *n*-hexane; see below) is tested in this work. The MCM is modified by kinetic and mechanistic information from the structure–activity relationships (SAR). Rate coefficients for the reactions of the dominant RO_2 with NO, unimolecular reactions of their alkoxy radicals,[32,33] as well as the organic nitrate yields of RO_2 radicals are replaced by the corresponding values predicted by SARs.[32,33,52,53] In addition, RO_2 isomerization reactions, which are not implemented in the MCM, are included as described in the SAR from Vereecken and Nozière.[54] Finally, the follow-up chemistry of newly formed RO_2 radicals is implemented as described by the SAR from Jenkin *et al.*[52] For *n*-hexane, the rates for unimolecular reactions of the alkoxy and alkylperoxy radical are provided by theoretical kinetics (Supporting Information Section D), reducing the uncertainty compared to general SAR predictions. This model is called MCM+SAR+THEO.

Additional modifications are implemented for some of the VOC species in the MCM+SAR mechanism to test whether the model–measurement agreement can be improved. These modifications are shown and discussed in Section 3. For *trans*-2-hexene, the reaction rate constant with O_3 is taken from Atkinson and Arey,[55] in agreement with results by Färber *et al.*[56]

2.5. Odd Oxygen (O_x) Production Rate. In this work, the production of odd oxygen ($O_x = O_3 + NO_2$) from the oxidation of different volatile organic compounds is investigated. The reactions of HO_2 and RO_2 radicals with NO produce NO_2 that subsequently forms ozone by its photolysis, while the reaction of OH with NO_2 forming nitric acid (HNO_3) is the predominant chemical loss of O_x[57] (Figure 1):

$$RO_2 + NO \rightarrow RO + NO_2 \quad (1)$$

$$RO_2 + NO + M \rightarrow RONO_2 + M \quad (2)$$

$$HO_2 + NO \rightarrow OH + NO_2 \quad (3)$$

$$OH + NO_2 + M \rightarrow HNO_3 + M \quad (4)$$

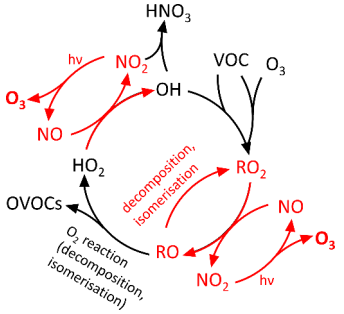

Figure 1. Schematic of the radical cycle initiated by the oxidation of the VOC by OH, leading to photochemical ozone production. Reactions leading to the formation of ozone are highlighted in red.

Besides Reaction 4, the formation of organic nitrates ($RONO_2$) from the reaction of RO_2 with NO terminates the radical cycle.[57]

The alkoxy radicals formed mainly in the reaction of RO_2 with NO (Reaction 1) can undergo either an H-abstraction reaction via the reaction with an oxygen molecule (Reaction 5) or unimolecular reactions, namely decomposition[32,53,58] (Reaction 6) and isomerization reactions[33] (Reaction 7):[59]

$$RO + O_2 \rightarrow R^1CHO + HO_2 \quad (5)$$

$$RO \rightarrow R^2 + R^3CHO \quad (6)$$

$$RO \rightarrow R^4 \quad (7)$$

https://doi.org/10.1021/acsestair.4c00064
ACS EST Air 2024, 1, 1096–1111

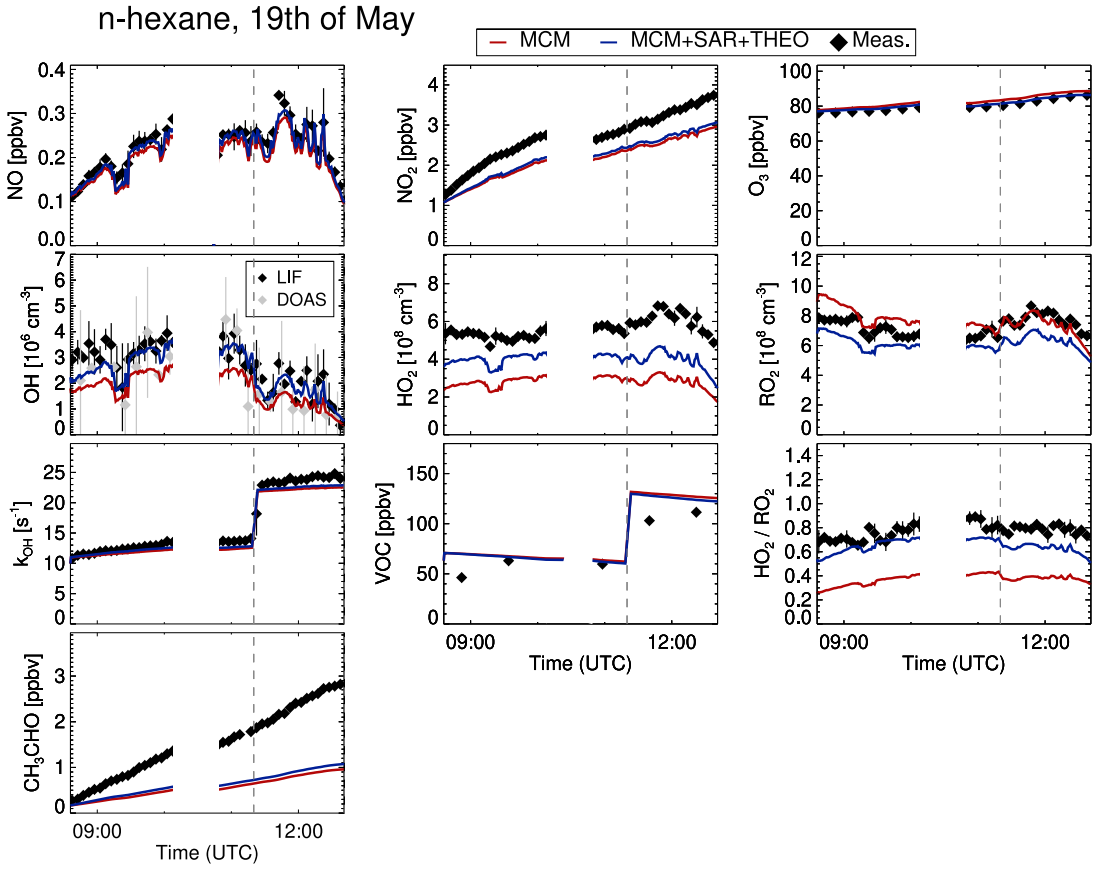

Figure 2. Comparison of measured and modelled radical and trace gas concentrations for the experiment with *n*-hexane at NO < 1 ppbv, performed on 19 May 2022. The vertical line indicates the second injection of the VOC into the chamber. Blue lines illustrate model results based on the MCM+SAR +THEO mechanism including theoretically calculated isomerization reaction rate coefficients for the first-generation alkoxy radicals and the isomerization products $C_2H_5CH(OH)C_2H_4CH_2OO^\bullet$ (MCM notation: HO3C6O2) and $CH_3CH(OH)C_2H_4CH(OO^\bullet)CH_3$ (MCM notation: HO2C6O2). More information about the theoretically calculated reaction rate coefficients can be found in the Supporting Information Section D.

H-abstraction reactions (Reaction 5) are common for alkoxy radicals formed from alkanes smaller than C_4 and for OH-substituted alkyl radicals often formed from β−OH-substituted alkoxy radical decomposition, e.g., in the oxidation of unsaturated VOCs such as alkenes, isoprene, and monoterpenes.[32,33,59] In contrast to the reaction with oxygen (Reaction 5), decomposition and isomerization reactions (Reactions 6 and 7) do not necessarily lead to the formation of HO_2. Instead, the alkyl radicals R^2 and R^4, the latter having a hydroxyl group at the former alkoxy site, react with O_2 forming another peroxy radical.[32,33,59] The newly formed RO_2 radical can react again with NO forming another alkoxy radical, which can undergo Reactions 5 to 7. In this way, more than two NO_2 molecules are formed for each RO_2 radical initially produced from the reaction of OH with the VOC.

In this work, two groups of VOCs were investigated: propane, propene, and *trans*-2-hexene, where the alkoxy radicals from the initial OH reaction produce HO_2 directly, and isopentane and *n*-hexane, where alkoxy radicals in their oxidation lead partly to the formation of another RO_2 radical by decomposition (isopentane) or isomerization (*n*-hexane) before HO_2 is produced. Simplified oxidation schemes of the investigated compounds can be found in the Supporting Information Section A (Figures S1−S5).

If information about radical and trace gas concentrations is available, the O_x production rate from Reactions 1−4 can be calculated.[60−62] In addition, also the following minor reactions, destroying ozone, were included, since the corresponding species were measured:

$$HO_2 + O_3 \rightarrow OH + 2O_2 \quad (8)$$

$$h\nu + O_3 \rightarrow O(^1D) + O_2 \quad (9)$$

$$\text{alkene} + O_3 \rightarrow \text{products} \quad (10)$$

The contributions of other reactions, such as the reaction of OH with ozone, are negligible. The O_x production rate from measured or modelled radical concentrations can then be derived according to

$$\begin{aligned} P(O_x)_{\text{radical}} = {} & k_{HO_2+NO}\cdot[HO_2][NO]\cdot(1 - f_{RONO_2}) \\ & + k_{HO_2+NO}\cdot[HO_2][NO] - k_{OH+NO_2} \\ & \cdot[OH][NO_2] - k_{HO_2+O_3}\cdot[HO_2][O_3] \\ & - f_{O(^1D)+H_2O} j_{O(^1D)}[O_3] - k_{O_3+\text{alkene}}[O_3] \\ & [\text{alkene}] \end{aligned} \quad (11)$$

where $f_{O(^1D)+H_2O}$ is the fraction of $O^1(D)$ reacting with water vapor (H_2O) forming OH and f_{RONO_2} denotes an averaged organic nitrate yield from the reaction of RO_2 with NO (Reaction 2). In this work, f_{RONO_2} was calculated from the modelled RO_2 distribution for each experiment and each

https://doi.org/10.1021/acsestair.4c00064
ACS EST Air 2024, 1, 1096−1111

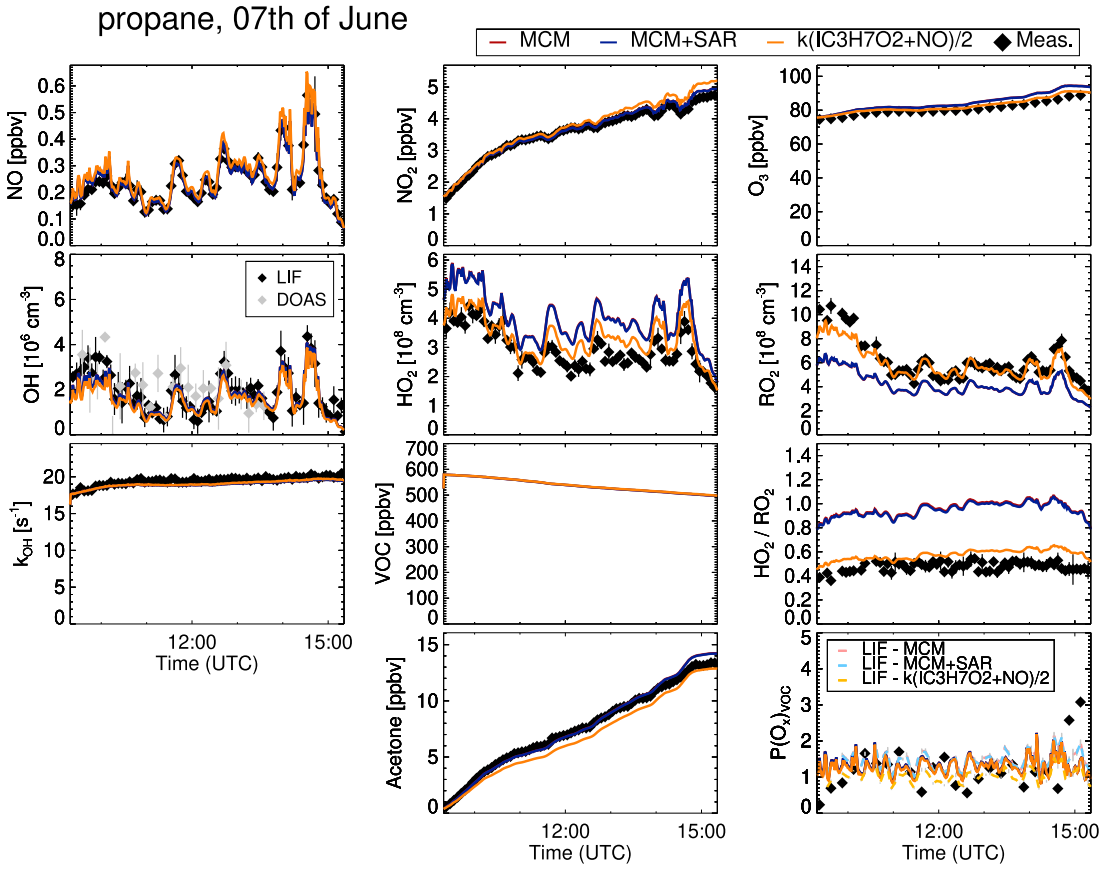

Figure 3. Comparison of measured and modelled trace gas concentrations for the experiment with propane at NO < 1 ppbv, performed on 7 June 2022. Orange lines illustrate model results from a test mechanism assuming a factor of two lower rate coefficient of the reaction of the RO_2 isoC$_3$H$_7$OO$^\bullet$ (MCM notation: IC3H7O2) with NO.

chemical mechanism individually, so that specific RO_2 radicals and their individual reaction with NO, including the yield of organic nitrate and NO_2, are accounted for. The rate coefficients k_{HO_2+NO} and $k_{HO_2+O_3}$ are taken from IUPAC[63] and k_{RO_2+NO} is taken from Jenkin et al.,[52] as these are also implemented in the MCM. The $P(O_x)_{radical}$ was determined from measured and modelled radical concentrations, $P(O_x)_{LIF}$ and $P(O_x)_{model}$, respectively. For NO > 1 ppbv, measured peroxy radical concentrations were not reliable to determine the O_x production rate $P(O_x)_{LIF}$ (Section 2.2).

In addition to using radical concentrations (eq 11), the O_x production rate can also be determined from the increase of the measured O_x concentration:

$$P(O_x)_{O_x} = \frac{d[O_x]}{dt} + k_{dilution}[O_x] + k_{wall}[O_x] \quad (12)$$

after correcting for dilution and for the loss of ozone to the chamber walls. With a loss rate of $\sim 1.5 \times 10^{-6}$ s^{-1} the impact of the wall loss of ozone on the O_x production rate $P(O_x)_{O_x}$ is negligible. Eq 12 is applicable for studies in atmospheric simulation chambers, in which transport processes do not play a role, so that only chemical sources and sinks and dilution determine the O_x concentration.

In this study, all O_x production rates are normalized to the rate of the reaction of OH with VOCs to ensure that values of the O_x production rate in the different experiments can be compared. The rate of the oxidation of VOCs by OH is given by the measured OH reactivity, corrected for species that do not form radicals and thus do not contribute to the O_x production:

$$L(OH + VOC) = (k_{OH} - k_{OH+NO_2}[NO_2] - k_{OH+NO}[NO])\cdot[OH] \quad (13)$$

In eq 13, the reactions of OH with NO_2 and with NO are included, as they lead to nitric acid and nitrous acid, respectively. The major OH reactants considered are the injected VOC, propanal, and acetaldehyde. Furthermore, the OH background reactivity is included, although it constitutes a small fraction of the total reactivity.

The O_x production per OH + VOC reaction, in the following called O_x production per oxidized VOC, $P(O_x)_{VOC}$, is then defined as

$$P(O_x)_{VOC} = P(O_x)/L(OH + VOC) \quad (14)$$

3. MODEL-MEASUREMENT COMPARISON

For most of the species investigated, negligible differences are obtained for NO, NO_2, and O_3 concentrations if either the MCM or the MCM+SAR chemical mechanism is applied for experiments at either low (<1 ppbv) or high (up to 9 ppbv) NO mixing ratios (Figures 2−5, S6−S12). A model−measurement agreement within 15% is found in all experiments, except for the experiments with *n*-hexane at low NO, where both mechanisms underestimate the measured NO_2 by 25% (Figure 2), and for the

https://doi.org/10.1021/acsestair.4c00064
ACS EST Air 2024, 1, 1096−1111

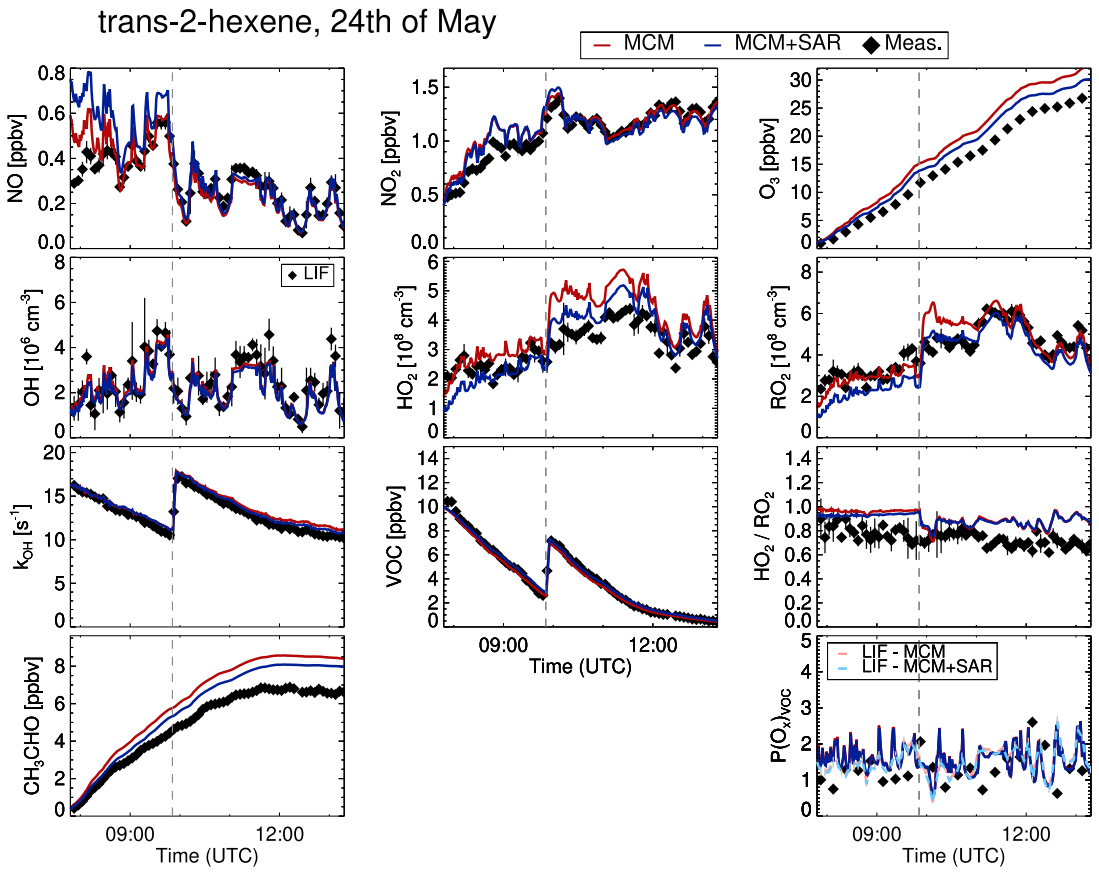

Figure 4. Comparison of measured and modelled trace gas concentrations for the experiment with *trans*-2-hexene at NO < 1 ppbv, performed on 24 May 2022. The vertical line indicates the second injection of the VOC into the chamber.

experiment with propene at high NO, where both mechanisms overestimate the O_3 by up to a factor of 1.25 (Figure S9).

The model results for OH radical concentrations and OH reactivity show negligible differences if either the MCM or the MCM+SAR mechanism is used. For all experiments at low NO (Figures 2−5, S6, S8, and S10), an excellent model−measurement agreement within the accuracy is found for the OH radical concentration, measured by the RO_xLIF instrument. At NO $\gtrsim$1 ppbv (Figures S7, S9, S11, and S12), model results have the tendency to underestimate both, the measured OH radical concentration and OH reactivity, though still an agreement within 35% is found for all species investigated. A good agreement is found between measured and modeled VOC mixing ratios (within 15%) with negligible differences between the MCM and the MCM+SAR mechanisms.

Overall, both mechanisms can reproduce measured HO_2 radical concentrations within 15% for experiments with propane (Figure 3), *trans*-2-hexene (Figure 4), and isopentane (Figure 5) at 0.3 < NO < 0.9 ppbv. An agreement within 30% is found for propene and isopentane at NO < 0.3 ppbv. For the experiment with *n*-hexane (Figure 2), the MCM model results underestimate the measured HO_2 by ∼50%. Applying the MCM+SAR +THEO mechanism gives an agreement within 32%. The better agreement observed for the MCM+SAR+THEO mechanism is mainly due to the additional RO_2 isomerization reactions of $C_2H_5CH(OH)C_3H_6OO^\bullet$ (MCM notation: HO3C6O2) and $CH_3CH(OH)C_2H_4CH(OO^\bullet)CH_3$ (MCM notation: HO2C6O2), forming HO_2, which outcompete the RO_2 reaction with NO. The competition between the isomerization reaction of $CH_3CH(OH)C_2H_4CH(OO^\bullet)CH_3$ (MCM notation: HO2C6O2) and its reaction with NO, in particular at elevated temperatures and low NO conditions, was already predicted by Praske et al.[11] Higher modelled HO_2 radical concentrations are reached as HO_2 is produced faster from the RO_2 isomerization reactions while the HO_2 loss rate does not change. In addition, the yield of organic nitrates of the two predominantly formed RO_2 radicals, $C_3H_7CH(OO^\bullet)C_2H_5$ (MCM notation: HEXCO2) and $C_4H_9CH(OO^\bullet)CH_3$ (MCM notation: HEXBO2), is lower in the MCM+SAR+THEO (16%) than in the MCM (∼22%).[52] However, the impact of the different organic nitrate yields in the MCM and the MCM+SAR+THEO is of minor importance, as it can be seen in the experiment at high NO (Figure S12) due to a similar HO_2 yield.

The lack of reliable measurements of HO_2 and RO_2 radicals at high NO makes it difficult to judge if other processes may have played a role. However, results of the MCM+SAR+THEO model run, showing an improved model−measurement agreement for HO_2 at low NO, suggest that using the nitrate yield as in the Jenkin et al. SAR[52] (16% for HEXAO2 and HEXBO2, Figure S4) improves the model−measurement agreement overall.

For modeled RO_2 radical concentrations for all VOCs, only small differences of $\lesssim$20% are observed between the MCM and MCM+SAR mechanisms, except for the propane experiment, where model results underestimate the measured RO_2 radical concentration by ∼40% (Figure 3). A better agreement (within ∼20%) can be achieved for the propane experiment, if the reaction rate coefficient between the major RO_2 species formed, $isoC_3H_7OO^\bullet$ (MCM notation: IC3H7O2), and NO is decreased by half (from 9×10^{-12} cm^3 s^{-1} to 4.5×10^{-12} cm^3

https://doi.org/10.1021/acsestair.4c00064
ACS EST Air 2024, 1, 1096−1111

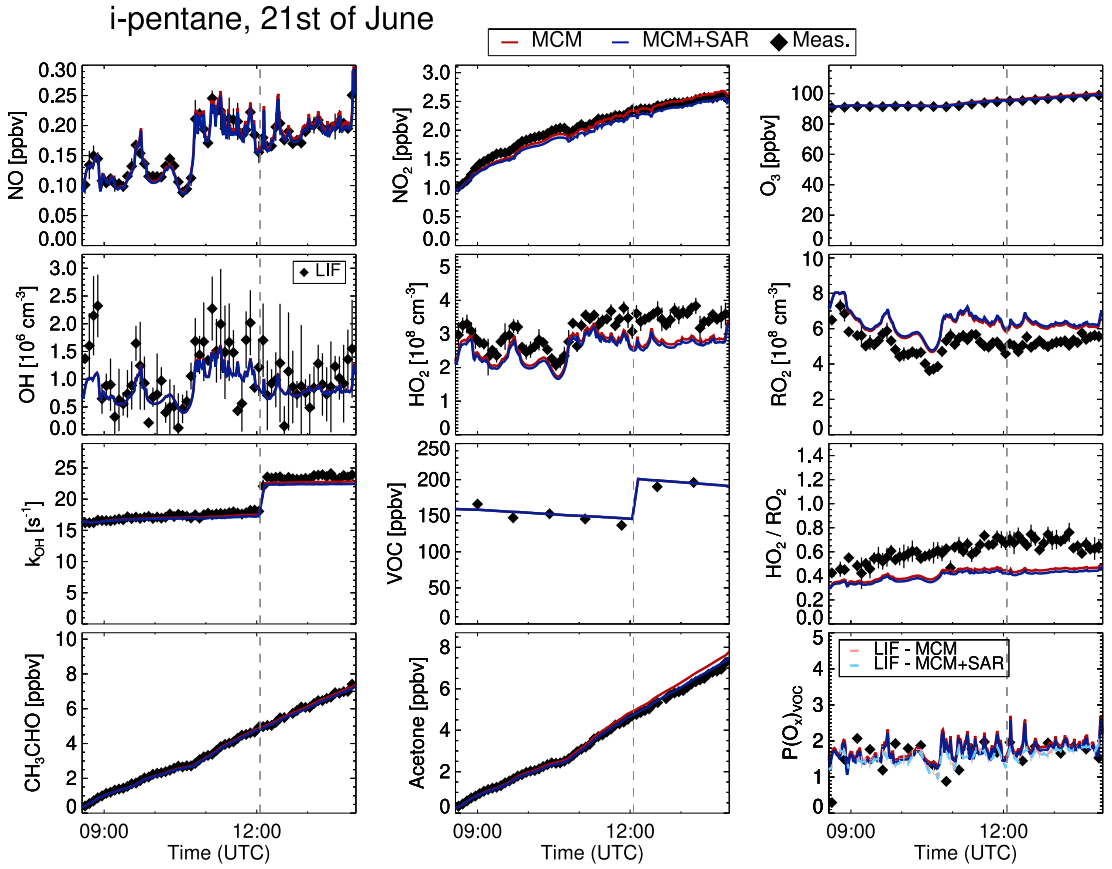

Figure 5. Comparison of measured and modelled trace gas concentrations for the experiment with isopentane at NO < 1 ppbv, performed on 21 June 2022. The vertical line indicates the second injection of the VOC into the chamber.

s^{-1} at 298 K) in the model. This is supported by previous studies by Adachi and Basco[64] and by Peeters *et al.*,[65] which suggest rate constants of $(3.5 \pm 0.3) \times 10^{-12}$ cm^3 s^{-1} and of $(5.0 \pm 1.2) \times 10^{-12}$ cm^3 s^{-1}, respectively, for the reaction of $isoC_3H_7OO^\bullet$ with NO. However, Eberhard *et al.*[66] suspected that results from Adachi and Basco[64] were affected by systematic errors caused by the formation of alkyl nitrites. Furthermore, measurements by Peeters *et al.*[65] needed to be corrected for contributions from secondary reactions and from organic nitrates.[66]

Acetone and/or acetaldehyde were measured in most experiments. Concentration time series are only shown in the figures if their production is not dominated by the production from the chamber wall but from the oxidation of the injected VOC. For most species investigated, good model−measurement agreement is observed at low NO (within 15%) with negligible differences between the different mechanisms (Figures 2−4, S6, S8, and S10). A slightly larger discrepancy of measurements and model results of 20 to 25% is observed in the experiment with *trans*-2-hexene at low NO, overestimating the measured acetaldehyde (Figure 4). Acetaldehyde is a major product of the oxidation of *trans*-2-hexene and is formed from the decomposition of the dominant (> 50%) first-generation alkoxy radicals produced, $C_3H_7CH(O^\bullet)CH(OH)CH_3$ (MCM notation: C65OH4O) and $C_3H_7CH(OH)CH(CH_3)O^\bullet$ (MCM notation: C64OH5O). Only decomposition reactions of these alkoxy radicals are considered in the MCM and the MCM+SAR mechanisms, with rate constants of 1×10^6 s^{-1} and 3.7×10^9 s^{-1} at 298 K, respectively. Isomerization reactions, which would yield another peroxy radical instead of the products acetaldehyde, butanal, and HO_2, are expected to proceed with reaction rate coefficients of 1×10^4 s^{-1} to 1×10^6 s^{-1} and are thus not competitive with the decomposition reaction, based on SAR-predicted rates.[32] Still, the discrepancy is within the accuracy of the instrument.

A larger model−measurement discrepancy is observed for acetaldehyde in the low NO experiment with *n*-hexane (Figure 2), with the MCM and the MCM+SAR+THEO mechanism underestimating the measurements by 70%. Uncertainties in the acetaldehyde concentrations, however, do not significantly affect the formation of PAN, which is expected to be a factor of 1.7 larger (equivalent to 70 pptv) when the model is constrained to measured values in the MCM+SAR+THEO model. Therefore, the effect on the O_x production is negligible.

For experiments with NO higher than 1 ppbv, an overestimation of the observed oxidation product concentrations (acetaldehyde in all experiments, acetone in the experiment with isopentane) by factors of 1.25 and ∼1.4 is seen for propene and isopentane, respectively, while measured acetaldehyde concentrations are underestimated by a factor of 1.5 by the MCM+SAR+THEO mechanism. In the case of isopentane, an increase of the organic nitrate yield of the first-generation RO_2, $C_2H_5C(CH_3)(CH_3)OO^\bullet$ (MCM notation: IPECO2) and $CH_3CH(CH_3)CH(CH_3)OO^\bullet$ (MCM notation: IPEBO2), formed in the oxidation of isopentane, may help improving the model−measurement agreement of the gas-phase products. A higher organic nitrate yield would result in less formation of the corresponding alkoxy radicals, which contribute significantly to the formation of acetone and acetaldehyde and thus would lead to a reduced formation of the aforementioned molecules. No

https://doi.org/10.1021/acsestair.4c00064
ACS EST Air 2024, 1, 1096−1111

data for products are available for the experiments with propane and *trans*-2-hexene.

In the case of propene, acetaldehyde is formed from the decomposition of the alkoxy radical $CH_3CH(O^•)CH_2(OH)$ (MCM notation: HYPROPO), formed from first generation RO_2. While no significant discrepancy was observed for NO < 1 ppbv (Figure S8), ~25% lower acetaldehyde concentrations were measured at high NO compared to the model results from the MCM and the MCM+SAR mechanism (Figure S9). The model−measurement discrepancy of up to 25% of the OH reactivity indicates that there might be compounds that are not included in the mechanisms and which do not contribute to the formation of acetaldehyde at the tested high NO conditions.

In summary, a good agreement (within the accuracy of measurements) is found for most measured species and, in particular, for OH, HO_2, and RO_2 radicals, when using the MCM+SAR mechanisms for all the VOCs investigated and for both low and high NO conditions. Negligible differences are found between the model results of the MCM and MCM+SAR mechanisms, with the exception of *n*-hexane, where a lower yield of nitrates in the MCM+SAR+THEO model, following the recommendation from the Jenkin et al. SAR,[52] improves the agreement between measured and modelled HO_2 radical and acetaldehyde concentrations. Furthermore, a better agreement between measured and modeled RO_2 radicals is found if the rate coefficient for the reaction of $isoC_3H_7OO^•$ (MCM notation: IC3H7O2) with NO was twice as low as currently implemented in the mechanisms and recommended by IUPAC.[67] Such a low value would be in agreement with previous studies by Adachi and Basco[64] and Peeters *et al.*[65] The overall good model−measurement agreement gives confidence in the ability of the mechanism used to correctly predict the radical concentrations and therefore also the ozone production, when used to analyze field data and/or to predict pollutant levels.

4. THE HO_2/RO_2 RADICAL CONCENTRATION RATIO

The HO_2/RO_2 radical concentration ratio observed in the experiments is expected to differ for VOCs producing alkoxy radicals with different chemistry. Figure 6 displays the HO_2/RO_2 radical concentration ratio averaged for the two VOC groups, forming HO_2 in one or two RO_2 radical reaction steps (Table 3, Table S1). Modelled HO_2/RO_2 radical concentration ratios are obtained using results from the MCM+SAR (MCM +SAR+THEO for *n*-hexane) chemical mechanism. For the averaging, only data are considered for which the injected VOC constitutes minimum 50% to the total OH reactivity. In the presence of a sufficiently high NO concentration like in the experiments performed in this study, it is anticipated that the production and the destruction rates of HO_2 and specific RO_2 radicals are very similar. This can be assumed, because the reaction rates of RO_2 and HO_2 with NO are comparable ($k = 9.0 \times 10^{-12}$ cm^3 s^{-1}[52] and $k = 8.4 \times 10^{-12}$ cm^3 s^{-1}[63] at 298 K, respectively). If HO_2 is formed from one RO_2 radical, this leads to a HO_2/RO_2 radical concentration ratio of approximately 1.

In contrast, if two RO_2 radical reaction steps are required because another intermediate RO_2 radical is formed by an isomerization or a decomposition reaction of the alkoxy radical, a larger total RO_2 radical concentration than HO_2 radical concentration is expected. Indeed, this is observed in the ratio of both, measured and modeled, radical concentrations in the experiments with VOCs that form such alkoxy radicals. In experiments with VOCs forming RO radicals which produce HO_2 after one RO_2 radical reaction step, the ratio is on average 0.9 for both, measured and modelled data, while in experiments with VOCs, forming RO radicals regenerating a RO_2 radical, an average ratio of 0.56 is observed for modelled and measured results (Figure 6).

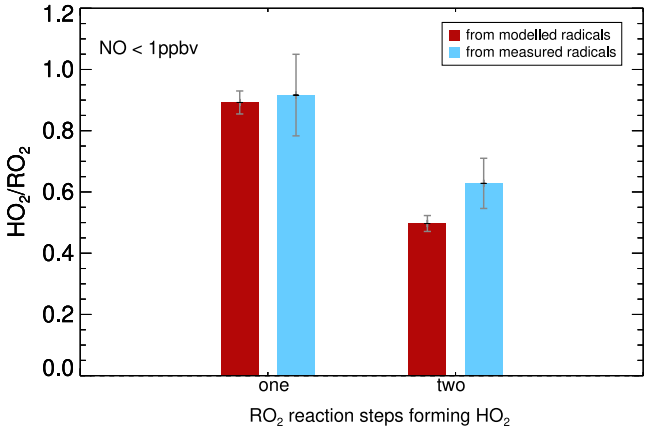

Figure 6. Comparison of HO_2/RO_2 radical concentration ratios, derived from modelled (MCM+SAR, MCM+SAR+THEO in case of *n*-hexane) and measured radical concentrations and averaged for the two groups of VOCs with different RO chemistry (Table 3, Figures S1−S5). Excluded are the experiments with propane, where measured radical concentrations could only be described by a factor of two lower RO_2 + NO reaction rate constants.

Table 3. Species Considered in the Calculation of the HO_2/RO_2 Radical Concentration Ratios and of the O_x Production Per Oxidized VOC[a]

		$P(O_x)_{VOC}$	
HO_2 formation	HO_2/RO_2	NO < 1 ppbv	NO > 1 ppbv
Single step	[b]	propane	propane
	propene	[c]	[d]
	trans-hexene	*trans*-2-hexene	[e]
Multistep	isopentane	isopentane	isopentane
	n-hexane	[f]	*n*-hexane

[a]Blank entries refer to species that were not considered in the analysis. Only data are considered for which the contribution of the VOC of interest to the total OH reactivity is more than 50%. [b]Not included because measurements could only be reproduced by assuming a factor of two smaller RO_2 + NO reaction rate constants which highly affects the HO_2/RO_2 radical concentration ratio. [c]No significant increase in O_x observed, resulting in a large uncertainty of the O_x production. [d]Contribution of propene to the total OH reactivity is less than 50% for 3 ppbv < NO < 6 ppbv. [e]No experiment available. [f]HO_2 is mainly formed from the isomerization of the regenerated RO_2, leading, at low NO, to an only small amount of peroxy radicals forming HO_2 in two NO reaction steps (Figure S4), and thus it cannot be grouped together with isopentane at these conditions.

5. ODD OXYGEN (O_X) PRODUCTION PER OXIDIZED VOC

Figure 7 shows the average odd oxygen production per oxidized VOC ($P(O_x)_{VOC}$) derived from measured radical concentrations ($P(O_x)_{VOC,LIF}$, eq 11), modelled (MCM+SAR) radical concentrations ($P(O_x)_{VOC,model}$, eq 11), as well as calculated from the

https://doi.org/10.1021/acsestair.4c00064
ACS EST Air 2024, 1, 1096−1111

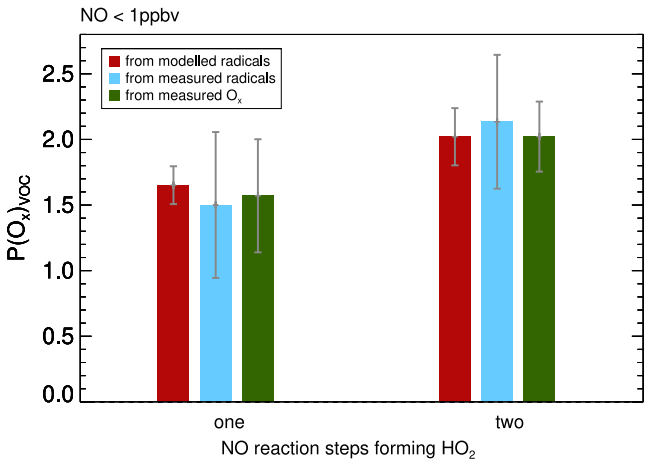

Figure 7. O_x production per oxidized VOC, derived from measured O_x concentrations, as well as from measured and modelled (MCM+SAR) radical concentrations and averaged for the two groups of VOCs with different RO chemistry (Table 3). Excluded are the experiments with propene, because of a too small increase in O_x, and with *n*-hexane, as the RO_2 isomerization dominates the loss of the regenerated RO_2 for NO < 1 ppbv (Figure S4).

measured O_x concentrations ($P(O_x)_{VOC,O_x}$, eq 12) (Section 2.5, Table S2). For the averaging, only data are considered for which the injected VOC constitutes minimum 50% to the total OH reactivity. The O_x production per oxidized VOC in Figure 7 are grouped according to the alkoxy chemistry of the VOC in the different experiments (Table 3). Similar as for the HO_2/RO_2 radical concentration ratio, the O_x production is expected to increase with the fraction of alkoxy radicals, regenerating RO_2 instead of producing HO_2. Values for times of the experiments, when NO was higher than 1 ppbv, were not included in the O_x production derived from measured radical concentrations as peroxy radical concentrations were in a similar range as the background signals (Section 2.2).

The O_x production per oxidized VOC, calculated from measured and modelled peroxy radical concentrations, $P(O_x)_{VOC,LIF}$, $P(O_x)_{VOC,model}$, and from the increase of the O_x concentrations, $P(O_x)_{VOC,O_x}$, overall agrees within the scatter around the averaged value (Figure 7). Unlike the calculation from measured radical concentrations ($P(O_x)_{VOC,LIF}$, eq 11), the determination from the O_x concentration increase, $P(O_x)_{VOC,O_x}$, is independent of the kinetics and the fate of the peroxy radicals and thus of the applied chemical model. The O_x production per oxidized VOC is on average ~25% higher for the VOCs, forming HO_2 in a single NO reaction-step, than for isopentane, producing HO_2 in a multi-step RO reaction. This is consistent with the expectation that another O_x molecule is formed in the reaction of the regenerated RO_2 with NO.

A comparison of different calculations of the O_x production, derived from experiments with NO < 1 ppbv (Figure 7) and from experiments with 3 ppbv < NO < 6 ppbv, is shown in Figure 8. Overall, the modeled O_x production shows a slight increase with increasing NO for both, one or two NO reaction steps before HO_2 is formed, which is within the statistical variability.

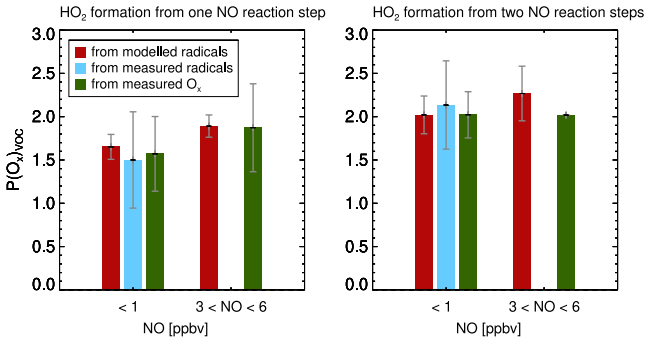

Figure 8. O_x production per oxidized VOC for NO < 1 ppbv and 3 ppbv < NO < 6 ppbv for VOCs forming RO which produce HO_2 either in one or in two NO reaction steps and averaged for the two groups of VOCs with different RO chemistry (Table 3, Figures S1–S5). Modelled normalized O_x production rates are based on the MCM +SAR mechanism and on the MCM+SAR+THEO mechanism for *n*-hexane.

6. DISCUSSION

Table 4 summarizes the HO_2/RO_2 radical concentration ratios, calculated from radical concentrations, measured in previous field campaigns[15−20] using laser-induced fluorescence instruments, and modelled radical concentrations using the MCM or the RACM. At low NO (< 1 ppbv), HO_2/RO_2 radical concentration ratios as low as 0.2 were observed in London,[16] north Norfolk,[20] and in Beijing in the summer.[15] In these studies, the ratios from modelled radical concentrations are by factors of up to 8 higher than the ratios obtained from measured radical concentrations.[15,20] At high NO (3 ppbv < NO < 6 ppbv), HO_2/RO_2 radical concentration ratios as low as 0.13−0.2

Table 4. Summary of Modeled and Measured HO_2/RO_2 Radical Concentration Ratios at Different NO Mixing Ratios, Found in Previous Field Studies and Observed in This Work[a]

	NO < 1 ppbv		3 < NO < 6 ppbv	
	$(HO_2/RO_2)_{meas}$	$(HO_2/RO_2)_{model}$	$(HO_2/RO_2)_{meas}$	$(HO_2/RO_2)_{model}$
Wangdu NCP[18]	0.9	1.3	0.3	1.7
BEST-ONE Beijing[17]	1.7	1.06	0.8	1.5
ClearfLo London[16]	0.2	0.6	0.2	1.1
AIRPRO Beijing winter[19]	–[b]	–[b]	0.25	1
AIRPRO Beijing summer[15]	0.2	1.4	0.13	1.25
ICOZA Norfolk[20]	0.25	2	0.6	–[c]
single-step HO_2 formation	0.92 ± 0.13	0.89 ± 0.04	–[d]	–[e]
multi-step HO_2 formation	0.63 ± 0.08	0.50 ± 0.02	–[d]	0.60 ± 0.02

[a]Model calculations are based on the MCM model,[15,16,19,20] the RACM base model[17,18] for the field data, or on MCM+SAR, for hexane MCM+SAR+THEO (results obtained from this study). Modeled and measured data were directly derived from the studies cited. For the value given for NO < 1 ppbv, minimum NO mixing ratios of 200 pptv were considered. [b]No data below NO = 1 ppbv. [c]No data for NO ≥3 ppbv. [d]The radical data was discarded for NO > 1 ppbv due to the low signal-to-background ratios of measurements (see Section 2.3 for details). [e]Contribution of propene to the total OH reactivity is less than 50% for 3 ppbv < NO < 6 ppbv.

https://doi.org/10.1021/acsestair.4c00064
ACS EST Air 2024, 1, 1096−1111

were also observed in Beijing[15,19] and in London.[16] Whereas the ratios calculated using the MCM are higher by a up to a factor of 10 in London,[16] the model overestimates the HO_2/RO_2 radical concentration ratios observed during the BEST-ONE campaign in Beijing[17] by only a factor of two. Overall, the model predicts HO_2/RO_2 radical concentration ratios larger than 1 for NO mixing ratios in the range of 3 ppbv to 6 ppbv, which is not in agreement with the measurements.

In the field studies performed in Wangdu in the North China Plain[18] and in London,[16] the VOCs investigated in this work (propane, propene, isopentane, *n*-hexane) contributed 15 to 20% to the total amount of measured non-methane VOCs. Propane, propene, and *n*-hexane were also observed during the AIRPRO campaign in Beijing.[15,19]

In this work, HO_2/RO_2 radical concentration ratios of ∼0.6 were found for VOCs forming HO_2 in two RO_2 radical reaction steps. This a factor of three larger than the value observed in London,[16] Beijing (summer),[15] and in north Norfolk[20] (Table 4). The much smaller HO_2/RO_2 ratios observed in the field studies would be explainable only if nearly all RO_2 radicals present in the field campaigns would undergo several NO reaction steps before forming a HO_2 radical. As this mechanism applies only for specific RO_2 species, it seems unlikely that this type of mechanism can explain the field observations. However, it cannot be excluded that there are so far unknown VOCs forming HO_2 in multiple RO_2 + NO reaction steps. The involved RO_2, however, must not be lost to reactions that do not regenerate a peroxy radical, such as the formation of organic nitrates or the formation of carbonyls from, e.g., the decomposition of OH-substituted alkyl radicals.

The HO_2/RO_2 radical concentration ratio observed in the chamber experiments for RO_2 radicals forming HO_2 in one RO_2 radical reaction step is similar to the ratio observed in Wangdu[28] (Table 4). However, in contrast to the results in the chamber experiments, modeled and measured radical concentrations disagreed, leading to an overestimation of the HO_2/RO_2 radical concentration ratio by the model.

In field campaigns in urban and close to urban areas, typical NO mixing ratios were between about 5 ppbv and 100 ppbv,[15,17−19] except for haze events in Beijing, when mixing ratios were much higher.[19] Radical measurements performed in London,[16] Beijing,[15,17,19] Wangdu,[18] and in north Norfolk, UK,[20] reveal a much higher O_x production rate derived from measured radical concentrations than derived from the model calculations (Table 5). While in Wangdu an agreement within ∼15% is found for NO < 1 ppbv,[18] modelled ozone production rates are found to be ∼50−75% lower than measured values in Beijing in the summer[15] and in north Norfolk.[20] Modelled rates are even up to a factor of 2.8 higher than measured values in London.[16] For NO mixing ratios between 3 and 6 ppbv, the model−measurement agreement of the ozone production rate worsens in most field studies (Table 5). The measured ozone production rate exceeds the modelled values by factors of up to 11 and 6 in north Norfolk[20] and in Beijing,[15,17,19] respectively, and by up to ∼2.2 in Wangdu.[18] Modelled and measured ozone production rates were in better agreement in London and Beijing in the summer, when the ratio of modeled and measured ozone production rates were between 0.5 and 0.7.

In contrast to observations in the field, a good agreement between modeled and measured ozone production is found in the experiments in this work (Table 5). Similar to the HO_2/RO_2 radical concentration ratio, the model−measurement agreement of the O_x production is comparable to the values observed in the field study in Wangdu[18] at NO < 1 ppbv. However, at high NO (3 ppbv < NO < 6 ppbv), the ozone production rate calculated from measured radical concentrations is three times larger than calculated from modelled values in Wangdu.[18] In the model, the majority of modeled RO_2 radicals produce HO_2 after one NO reaction step. However, if a larger fraction of RO_2 required two NO reaction steps, the expected ozone production rate would be still lower than calculated from measured radical concentration, as experiments in this work show that the ozone production would only increase by approximately 25% for the anthropogenic VOCs investigated.

Table 5. Summary of O_3 Production Rates, Determined in Previous Field Studies from Modeled $(P(O_3)_{model})$ and Measured $(P(O_3)_{LIF})$ Radical Concentrations[a]

	$P(O_3)_{model}/P(O_3)_{LIF}$	
	NO < 1 ppbv	3 < NO < 6 ppbv
Wangdu NCP[18]	0.9	0.36
BEST-ONE Beijing[17]	2	0.17
ClearfLo London[16]	2.8	0.7
AIRPRO Beijing winter[19]	−[b]	0.3
AIRPRO Beijing summer[15,c]	0.25	0.5
ICOZA Norfolk[20,c]	0.5	0.1
single-step HO_2 formation[c]	1.1 ± 0.4	1.00 ± 0.17[d]
multi-step HO_2 formation[c]	0.95 ± 0.25	replaced 1.10 ± 0.21 1.14 ± 0.16[d]

[a]Modeled radical concentrations are based on the MCM[15,16,19,20] or on the RACM base model[17,18] for the field data, and on MCM+SAR, for hexane MCM+SAR+THEO (results obtained from this study). Modeled and measured data were directly derived from the cited studies. For NO < 1 ppbv, minimum NO mixing ratios of 200 pptv were considered to better compare with the chemical conditions in this study. [b]No data below NO = 1 ppbv. [c]Values correspond to O_x production rates. [d]$P(O_x)_{VOC,model}/P(O_x)_{VOC,O_x}$.

Overall, the model−measurement discrepancy of 30 to 90% of the O_x production rate observed in the field campaigns cannot be reproduced in the chamber experiments investigating the oxidation of representative VOCs neither at low NO (< 1 ppbv) nor at higher NO (3 < NO < 6 ppbv, Table 5). Furthermore, no significant model−measurement discrepancy evolves for VOCs forming RO radicals which regenerate RO_2, making the multi-step HO_2 formation an unlikely candidate for explaining the observed discrepancies in the field campaigns. It should be noted, though, that the VOCs investigated, having rather simple chemical structures, represent a subset of the air mixtures observed in field studies and thus cannot be seen as a complete surrogate of ambient air.

Different attempts have been made to improve the model−measurement agreement of radical concentrations. Whalley *et al.*[15] found that the model−measurement discrepancy of the HO_2 and RO_2 radical concentration, and thus of the O_x production rate, can be improved by assuming the formation of a specific RO_2 radical $CH_3C(=O)CHCH_2CH(CH_2OO^{\bullet})$-$C(CH_3)CH_3$ (MCM notation: C96O2), a peroxy radical formed in the oxidation of α-pinene that produces HO_2 after four NO reaction steps. Even though one may expect a linear increase of the O_x production rate with the number of NO reactions steps per oxidized VOC, radical termination reactions, such as the decomposition of OH-substituted alkyl radicals formed in the isomerization of OH-containing RO_2 radicals and

https://doi.org/10.1021/acsestair.4c00064
ACS EST Air 2024, 1, 1096−1111

the formation of organic nitrates from the reaction of RO_2 with NO (eq 2) limit the O_x production rate.

To assess the impact of the organic nitrate yield on the O_x production rate, a steady-state analysis using a box model with a simplified chemical mechanism is performed. In the model, the fraction of the initially formed RO_2 radical which requires two NO reaction steps to form HO_2 is variable. In the zero-dimensional box model calculations, constant mixing ratios of NO and ozone of 2 ppbv and 50 ppbv, respectively, and a constant production rate of a R^1O_2 radical of 5 s^{-1} from the reaction of OH with an artificial VOC (X) are assumed. HO_2 is then formed after either one or two reaction steps with NO:

$$OH + X \rightarrow R^1O_2 \quad (15)$$

$$R^1O_2 + NO \xrightarrow{k_{RO_2+NO}\times(1-\mathbf{f}_{RONO_2})} R^1O + NO_2 \quad (16)$$

$$R^1O \xrightarrow{k_{O_2}} HO_2 + R'CHO \quad (17)$$

$$R^1O \xrightarrow{k_{uni}} R^2O_2 \quad (18)$$

$$R^2O_2 + NO \xrightarrow{k_{RO_2+NO}\times(1-\mathbf{f}_{RONO_2})} R^2O + NO_2 \quad (19)$$

$$R^2O \xrightarrow{k_{O_2}} HO_2 + R^{2'}CHO \quad (20)$$

where $\mathbf{f}_{RONO_2}$ is the organic nitrate yield, while k_{RO_2+NO}, k_{O_2}, and k_{uni} are rate constants of the reaction of RO_2 with NO, of RO with O_2[68] (pseudo-first order), and of unimolecular reactions of the alkoxy radical regenerating RO_2, respectively. If the nitrate yield is small ($\mathbf{f}_{RONO_2} \ll 1$) and all R^1O_2 form another RO_2 radical (i.e., $k_{uni} \gg k_{O_2}$), an approximately 55% higher O_x production is obtained as compared to a chemical system where RO_2 produces HO_2 after one NO reaction (i.e., $k_{uni} \ll k_{O_2}$, Figure 9) due to additionally produced NO_2 (O_x) from the

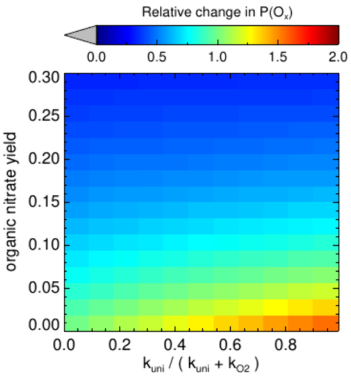

Figure 9. Results from steady-state model calculations for the dependence of the O_x production rate on the organic nitrate yield from the reaction of a RO_2 radical with NO and on the fraction of RO_2 in which RO undergo unimolecular reactions regenerating RO_2 such that HO_2 is formed in two RO_2 + NO reaction steps (Reactions 16−20). See text for details.

second RO_2 + NO reaction (Reaction 19). With increasing organic nitrate yield, the effect becomes smaller as the formation of organic nitrates terminates the radical chain before NO is oxidized to NO_2 in the reaction with another peroxy radical. The formation of organic nitrates nearly completely compensates the ozone production from the second NO reaction step for a nitrate yield higher than 20%. According to the SAR by Jenkin *et al.*,[52] the organic nitrate yield scales nonlinearly with the number of carbon atoms in the peroxy radical and can reach values up to 30%. For peroxy radicals with more than four carbon atoms, the RO_2 isomerization reaction competes at low NO conditions with the reaction of RO_2 with NO forming organic nitrates.

In the case of the RO_2 radical reactions following the reaction of NO with $CH_3C(=O)CHCH_2CH(CH_2OO^\bullet)C(CH_3)CH_3$ (MCM notation: C96O2), used in the sensitivity study by Whalley *et al.*,[15] the organic nitrate yield of the peroxy radical reactions with NO range between 0 and 16% in the MCM. In this case, the steady-state model would give an increase in the O_x production rate by a factor of 1.75. However, organic nitrate yields, implemented in the MCM, are up to 60% smaller than organic nitrate yields in the recent SAR by Jenkin *et al.*,[52] so that the increase in the ozone production from the additional NO reaction steps is likely less. For example, the organic nitrate yield for the peroxy radical $CH_3C(=O)C(OO^\bullet)CH_2CH(CH_2OH)$-$C(CH_3)CH_3$ (MCM notation: C97O2) formed in the subsequent chemistry of peroxy radical $CH_3C(=O)$-$CHCH_2CH(CH_2OO^\bullet)C(CH_3)CH_3$ (MCM notation: C96O2) is zero, although this is only expected for acyl ($R(=)OO^\bullet$) or aromatic peroxy radicals in the SAR.[52]

Overall, using the organic nitrate yields of the Jenkin et al. SAR[52] instead of the MCM, the impact of the conversion of alkoxy radicals to another RO_2 radical instead of HO_2 is strongly reduced, highlighting the organic nitrate yield being a limiting factor for the O_x production. Organic nitrate yields in the MCM may need to be updated to the most recent values from the SAR.[52] In addition, more experimental studies to determine organic nitrate yields would help to make more accurate predictions of the ozone production rates from the oxidation of specific organic compounds. Furthermore, RO_2 isomerization reactions, which can also limit the O_x production by forming a carbonyl and an HO_2 radical, are also not implemented in the MCM for the majority of RO_2 radicals. Considering those reactions can impact the O_x production from large RO_2 radicals significantly at low NO mixing ratios.

7. SUMMARY AND CONCLUSIONS

In this work, the chemical degradation of short and long-chain saturated linear (propane, *n*-hexane), branched (isopentane), and unsaturated (propene and *trans*-2-hexene) hydrocarbons by the OH radical were studied. The compounds were chosen as they are commonly observed in urban environments[16,29−31] from traffic emissions,[5,29] and they are also emitted as volatile chemical products, which can play a major role in urban environments.[29,69−71] These VOCs form alkoxy radicals characterized by different reaction pathways: (1) propane, propene, and *trans*-2-hexene form RO_2 radicals which produce HO_2 in one reaction step with NO, while (2) first-generation RO_2 radicals from isopentane and *n*-hexane require one to two NO reaction steps, regenerating another RO_2 radical in the process. In total, 11 experiments were performed in the outdoor atmospheric simulation chamber SAPHIR at Forschungszentrum Jülich, Germany, at NO mixing ratios between 0.1 ppbv and 9 ppbv. Zero-dimensional box model calculations were conducted and results were compared to measured trace gas and radical concentrations. For each compound, the chemical mechanism MCM+SAR was used which is based on the MCM and updated and complemented with reaction rate coefficients and reaction pathways derived from SAR for the predominantly formed peroxy radicals[52,54] and the alkoxy

https://doi.org/10.1021/acsestair.4c00064
ACS EST Air 2024, 1, 1096−1111

radicals[32,33] and, for *n*-hexane, theoretical kinetic calculations. Overall, a good model−measurement agreement, particularly of the OH, HO_2, and RO_2 radical concentrations, is found for most of the investigated species. Differences between model results using the MCM and the MCM+SAR mechanisms are small, except for *n*-hexane, for which measured radicals are better described by the MCM+SAR+THEO mechanism. In this case, the major update of the MCM+SAR+THEO mechanism are additional isomerization reactions of the RO_2 radicals as well as modified organic nitrate yields for the major RO_2 radicals formed. For propane, HO_2 and RO_2 radical concentrations are reproduced best, if a factor of two slower rate coefficient of the reaction of $isoC_3H_7OO^\bullet$ (MCM notation: IC3H7O2) with NO is used in agreement with results of Adachi and Basco[64] and Peeters *et al.*[65]

The impact of alkoxy radical isomerization reactions on the radicals and ozone production was assessed by investigating the HO_2/RO_2 radical concentration ratio as well as the O_x production per VOC oxidized by OH. In field studies such as in London,[16] Beijing,[15,17,19] Wangdu,[18] and north Norfolk,[20] significant model−measurement discrepancies were found for HO_2 and RO_2 radical concentrations. In all campaigns, the models tend to underestimate the measured radical concentrations with increasing NO concentrations. As a consequence, the O_x production rate calculated from the measured radical concentrations is higher (up to a factor of 100 in Beijing[15]) than from modelled concentrations. In the experiments in this study, a ∼40% lower HO_2/RO_2 radical concentration ratio is found for VOCs (isopentane and *n*-hexane) producing RO radicals which require two NO reaction steps instead of only one to form an HO_2 radical. In contrast, a more than two times larger HO_2/RO_2 radical concentration ratio was observed in field campaigns in London,[16] Beijing,[15] and north Norfolk,[20] so that the unexpected low ratio cannot be explained by the presence of this type of RO_2 formed from the oxidation of unmeasured organic compounds. For the experiments in this work, the O_x production per oxidized organic compound was determined from using (1) modelled radical concentrations, $P(O_x)_{VOC,model}$, (2) measured radical concentrations, $P(O_x)_{VOC,LIF}$, and (3) the change of the measured O_x concentrations, $P(O_x)_{VOC,O_x}$. Overall, a good agreement within 15% is observed for the different approaches at low (NO < 1 ppbv) and high NO (3 < NO < 6 ppbv), whereby for the latter case, the O_x production from measured radicals could not be determined. The production of O_x from isopentane, producing peroxy radicals forming HO_2 in two RO_2+NO reaction steps, was found to be 27% larger than that for propane and *trans*-2-hexene, forming RO radicals which directly produce HO_2.

The model−measurement discrepancies found in field campaigns in Beijing in the summer[15] and in north Norfolk[20] in London[16] and in Beijing in winter[17] were much higher. Based on the present knowledge, the additional O_x production required to explain the observations seems to be unlikely due to reactions of RO_2 species that require two NO reaction steps to form an HO_2 radical and are produced from unmeasured VOCs not included in the model calculations. Other explanations for the model−measurement discrepancies found in the field have been suggested in the literature, for example the oxidation of VOCs by chlorine which would lead to an increased radical production. Overall, the model−measurement discrepancies observed in the different field studies cannot be understood with the current knowledge and further investigations are needed.

■ ASSOCIATED CONTENT

Data Availability Statement

Data from the experiments in the SAPHIR chamber used in this work are available on the EUROCHAMP data home page (https://data.eurochamp.org/). Experiments with propane performed at NO < 1 ppbv and NO > 1 ppbv are available at DOI: 10.25326/PVYS-HR72[72] (13 May 2022), DOI: 10.25326/A5ZM-W179[73] (07 June 2022), and DOI: 10.25326/A742-9J73[74] (18 May 2022), respectively. Experimental data from the photooxidation oxidation experiments of propene in the presence of NO < 1 ppbv and NO > 1 ppbv are accessible at DOI: 10.25326/B0ZW-YQ76[75] (09 June 2022) and DOI: 10.25326/0T20-XY65[76] (23 June 2022), respectively. Data from the photooxidation experiment of *trans*-2-hexene at NO < 1 ppbv is available at DOI: 10.25326/P6Q8-0N05[77] (24 May 2022). Experiments with isopentane in the presence of NO < 1 ppbv and NO > 1 ppbv are available at DOI: 10.25326/ZQHP-BA18[78] (21 June 2022), DOI: 10.25326/A5RG-3327[79] (11 June 2022), and DOI: 10.25326/87E2-JF37[80] (16 June 2022), respectively. Data from the photooxidation experiments of *n*-hexane at NO < 1 ppbv and NO > 1 ppbv are available at DOI: 10.25326/QJYB-JW72[81] (19 May 2022) and DOI: 10.25326/2GGT-JY88[82] (22 May 2022), respectively. The raw quantum chemical data of the theoretical kinetic study of selected alkoxy and peroxy radicals formed in the photooxidation of *n*-hexane is available under DOI: 10.26165/JUELICH-DATA/J2LHTQ.[83]

Supporting Information

The Supporting Information is available free of charge at https://pubs.acs.org/doi/10.1021/acsestair.4c00064.

Figures S1−S13, Tables S1−S3, OH reaction schemes of compounds investigated in this work, model−measurement comparison plots of further experiments, overview of modelled and measured HO_2/RO_2 radical concentration ratios and of derived $P(O_x)$, a theoretical kinetic study of the key alkoxy and peroxy radicals in the *n*-hexane system (PDF)

■ AUTHOR INFORMATION

Corresponding Authors

Hendrik Fuchs − *Institute for Energy and Climate Research, IEK-8: Troposphere, Forschungszentrum Jülich GmbH, 52425 Jülich, Germany; Department of Physics, University of Cologne, 50937 Cologne, Germany;* orcid.org/0000-0003-1263-0061; Email: h.fuchs@fz-juelich.de

Anna Novelli − *Institute for Energy and Climate Research, IEK-8: Troposphere, Forschungszentrum Jülich GmbH, 52425 Jülich, Germany*; Email: a.novelli@fz-juelich.de

Authors

Michelle Färber − *Institute for Energy and Climate Research, IEK-8: Troposphere, Forschungszentrum Jülich GmbH, 52425 Jülich, Germany;* orcid.org/0009-0003-0302-6142

Birger Bohn − *Institute for Energy and Climate Research, IEK-8: Troposphere, Forschungszentrum Jülich GmbH, 52425 Jülich, Germany;* orcid.org/0000-0003-4177-3934

Philip T. M. Carlsson − *Institute for Energy and Climate Research, IEK-8: Troposphere, Forschungszentrum Jülich GmbH, 52425 Jülich, Germany;* orcid.org/0000-0002-5365-1689

Georgios I. Gkatzelis − *Institute for Energy and Climate Research, IEK-8: Troposphere, Forschungszentrum Jülich*

https://doi.org/10.1021/acsestair.4c00064
ACS EST Air 2024, 1, 1096−1111

GmbH, 52425 Jülich, Germany; orcid.org/0000-0002-4608-3695

Andrea C. Marcillo Lara − *Institute for Energy and Climate Research, IEK-8: Troposphere, Forschungszentrum Jülich GmbH, 52425 Jülich, Germany*

Franz Rohrer − *Institute for Energy and Climate Research, IEK-8: Troposphere, Forschungszentrum Jülich GmbH, 52425 Jülich, Germany*

Luc Vereecken − *Institute for Energy and Climate Research, IEK-8: Troposphere, Forschungszentrum Jülich GmbH, 52425 Jülich, Germany;* orcid.org/0000-0001-7845-684X

Sergej Wedel − *Institute for Energy and Climate Research, IEK-8: Troposphere, Forschungszentrum Jülich GmbH, 52425 Jülich, Germany*

Andreas Wahner − *Institute for Energy and Climate Research, IEK-8: Troposphere, Forschungszentrum Jülich GmbH, 52425 Jülich, Germany*

Complete contact information is available at: https://pubs.acs.org/10.1021/acsestair.4c00064

Notes

The authors declare no competing financial interest.

REFERENCES

(1) *Air Quality in Europe. EEA Report*; European Environment Agency, 2020; p 9.

(2) Gakidou, E.; et al. Global, regional, and national comparative risk assessment of 84 behavioural, environmental and occupational, and metabolic risks or clusters of risks, 1990 − 2016: a systematic analysis for the Global Burden of Disease Study 2016. *Lancet* **2017**, *390*, 1345−1422.

(3) Seinfield, J. H.; Pandis, S. *Atmospheric Chemistry and Physics: From Air Pollution to Climate Change*; Wiley, 2006.

(4) Pollack, I. B.; Ryerson, T. B.; Trainer, M.; Neuman, J. A.; Roberts, J. M.; Parrish, D. D. Trends in ozone, its precursors, and related secondary oxidation products in Los Angeles, California: A synthesis of measurements from 1960 to 2010. *J. Geophys. Res. Atmos.* **2013**, *118*, 5893−5911.

(5) Ehlers, C.; Klemp, D.; Rohrer, F.; Mihelcic, D.; Wegener, R.; Kiendler-Scharr, A.; Wahner, A. Twenty years of ambient observations of nitrogen oxides and specified hydrocarbons in air masses dominated by traffic emissions in Germany. *Faraday Discuss.* **2016**, *189*, 407−437.

(6) Li, K.; Jacob, D. J.; Liao, H.; Shen, L.; Zhang, Q.; Bates, K. H. Anthropogenic drivers of 2013−2017 trends in summer surface ozone in China. *Proc. Natl. Acad. Sci. U.S.A.* **2019**, *116*, 422−427.

(7) Warneke, C.; De Gouw, J. A.; Holloway, J. S.; Peischl, J.; Ryerson, T. B.; Atlas, E.; Blake, D.; Trainer, M.; Parrish, D. D. Multiyear trends in volatile organic compounds in Los Angeles, California: Five decades of decreasing emissions. *J. Geophys. Res. Atmos.* **2012**, *117*, D00V17.

(8) Li, K.; et al. Ozone pollution in the North China Plain spreading into the late-winter haze season. *Proc. Natl. Acad. Sci. U.S.A.* **2021**, *118*, No. e2015797118.

(9) Jiang, Z.; McDonald, B. C.; Worden, H.; Worden, J. R.; Miyazaki, K.; Qu, Z.; Henze, D. K.; Jones, D. B. A.; Arellano, A. F.; Fischer, E. V.; Zhu, L.; Boersma, K. F. Unexpected slowdown of US pollutant emission reduction in the past decade. *Proc. Natl. Acad. Sci. U.S.A.* **2018**, *115*, 5099−5104.

(10) Coggon, M. M.; et al. Volatile chemical product emissions enhance ozone and modulate urban chemistry. *Proc. Natl. Acad. Sci. U.S.A.* **2021**, *118*, No. e2026653118.

(11) Praske, E.; Otkjær, R. V.; Crounse, J. D.; Hethcox, J. C.; Stoltz, B. M.; Kjaergaard, H. G.; Wennberg, P. O. Atmospheric autoxidation is increasingly important in urban and suburban North America. *Proc. Natl. Acad. Sci. U.S.A.* **2018**, *115*, 64−69.

(12) Goldman, M. J.; Green, W. H.; Kroll, J. H. Chemistry of Simple Organic Peroxy Radicals under Atmospheric through Combustion Conditions: Role of Temperature, Pressure, and NO_x Level. *J. Phys. Chem. A* **2021**, *125*, 10303−10314.

(13) Brune, W.; et al. Urban case studies: general discussion. *Faraday Discuss.* **2016**, *189*, 473−514.

(14) Griffith, S. M.; et al. Measurements of hydroxyl and hydroperoxy radicals during CalNex-LA: Model comparisons and radical budgets. *J. Geophys. Res. Atmos.* **2016**, *121*, 4211−4232.

(15) Whalley, L. K.; et al. Evaluating the sensitivity of radical chemistry and ozone formation to ambient VOCs and NO_x in Beijing. *Atmos. Chem. Phys.* **2021**, *21*, 2125−2147.

(16) Whalley, L. K.; Stone, D.; Dunmore, R.; Hamilton, J.; Hopkins, J. R.; Lee, J. D.; Lewis, A. C.; Williams, P.; Kleffmann, J.; Laufs, S.; Woodward-Massey, R.; Heard, D. E. Understanding in situ ozone production in the summertime through radical observations and modelling studies during the Clean air for London project (ClearfLo). *Atmos. Chem. Phys.* **2018**, *18*, 2547−2571.

(17) Tan, Z.; et al. Wintertime photochemistry in Beijing: observations of RO_x radical concentrations in the North China Plain during the BEST-ONE campaign. *Atmos. Chem. Phys.* **2018**, *18*, 12391−12411.

(18) Tan, Z.; et al. Radical chemistry at a rural site (Wangdu) in the North China Plain: observation and model calculations of OH, HO_2 and RO_2 radicals. *Atmos. Chem. Phys.* **2017**, *17*, 663−690.

(19) Slater, E. J.; et al. Elevated levels of OH observed in haze events during wintertime in central Beijing. *Atmos. Chem. Phys.* **2020**, *20*, 14847−14871.

(20) Woodward-Massey, R.; et al. Radical chemistry and ozone production at a UK coastal receptor site. *Atmos. Chem. Phys.* **2023**, *23*, 14393−14424.

(21) Jenkin, M. E.; Saunders, S. M.; Pilling, M. J. The tropospheric degradation of volatile organic compounds: a protocol for mechanism development. *Atmos. Environ.* **1997**, *31*, 81−104.

(22) Saunders, S. M.; Jenkin, M. E.; Derwent, R. G.; Pilling, M. J. Protocol for the development of the Master Chemical Mechanism, MCM v3 (Part A): tropospheric degradation of non-aromatic volatile organic compounds. *Atmos. Chem. Phys.* **2003**, *3*, 161−180.

(23) Goliff, W. S.; Stockwell, W. R.; Lawson, C. V. The regional atmospheric chemistry mechanism, version 2. *Atmos. Environ.* **2013**, *68*, 174−185.

(24) Dusanter, S.; Vimal, D.; Stevens, P. S.; Volkamer, R.; Molina, L. T. Measurements of OH and HO_2 concentrations during the MCMA-2006 field campaign − Part 1: Deployment of the Indiana University laser-induced fluorescence instrument. *Atmos. Chem. Phys.* **2009**, *9*, 1665−1685.

(25) Fuchs, H.; Bohn, B.; Hofzumahaus, A.; Holland, F.; Lu, K. D.; Nehr, S.; Rohrer, F.; Wahner, A. Detection of HO_2 by laser-induced fluorescence: calibration and interferences from RO_2 radicals. *Atmos. Meas. Technol.* **2011**, *4*, 1209−1225.

(26) Whalley, L. K.; Blitz, M. A.; Desservettaz, M.; Seakins, P. W.; Heard, D. E. Reporting the sensitivity of laser-induced fluorescence instruments used for HO_2 detection to an interference from RO_2 radicals and introducing a novel approach that enables HO_2 and certain RO_2 types to be selectively measured. *Atmos. Meas. Technol.* **2013**, *6*, 3425−3440.

(27) Lu, K. D.; et al. Observation and modelling of OH and HO_2 concentrations in the Pearl River Delta 2006: a missing OH source in a VOC rich atmosphere. *Atmos. Chem. Phys.* **2012**, *12*, 1541−1569.

(28) Tan, Z.; et al. Experimental budgets of OH, HO_2, and RO_2 radicals and implications for ozone formation in the Pearl River Delta in China 2014. *Atmos. Chem. Phys.* **2019**, *19*, 7129−7150.

(29) McDonald, B. C.; et al. Volatile chemical products emerging as largest petrochemical source of urban organic emissions. *Science* **2018**, *359*, 760−764.

(30) Lu, X.; Chen, N.; Wang, Y.; Cao, W.; Zhu, B.; Yao, T.; Fung, J. C. H.; Lau, A. K. H. Radical budget and ozone chemistry during autumn in the atmosphere of an urban site in central China. *J. Geophys. Res. Atmos.* **2017**, *122*, 3672−3685.

(31) Zhao, Q.; Bi, J.; Liu, Q.; Ling, Z.; Shen, G.; Chen, F.; Qiao, Y.; Li, C.; Ma, Z. Sources of volatile organic compounds and policy

implications for regional ozone pollution control in an urban location of Nanjing, East China. *Atmos. Chem. Phys.* **2020**, *20*, 3905−3919.
(32) Vereecken, L.; Peeters, J. Decomposition of substituted alkoxy radicals—part I: a generalized structure−activity relationship for reaction barrier heights. *Phys. Chem. Chem. Phys.* **2009**, *11*, 9062−9074.
(33) Vereecken, L.; Peeters, J. A structure−activity relationship for the rate coefficient of H-migration in substituted alkoxy radicals. *Phys. Chem. Chem. Phys.* **2010**, *12*, 12608−12620.
(34) Rohrer, F.; Bohn, B.; Brauers, T.; Brüning, D.; Johnen, F.-J.; Wahner, A.; Kleffmann, J. Characterisation of the photolytic HONO-source in the atmosphere simulation chamber SAPHIR. *Atmos. Chem. Phys.* **2005**, *5*, 2189−2201.
(35) Schlosser, E.; Bohn, B.; Brauers, T.; Dorn, H.-P.; Fuchs, H.; Hässler, R.; Hofzumahaus, A.; Holland, F.; Rohrer, F.; Rupp, L.-O.; Siese, M.; Tillmann, R.; Wahner, A. Intercomparison of Two Hydroxyl Radical Measurement Techniques at the Atmosphere Simulation Chamber SAPHIR. *J. Atmos. Chem.* **2007**, *56*, 187−205.
(36) Fuchs, H.; et al. Technical Note: Formal blind intercomparison of HO_2 measurements in the atmosphere simulation chamber SAPHIR during the HOxComp campaign. *Atmos. Chem. Phys.* **2010**, *10*, 12233−12250.
(37) Apel, E. C.; et al. Intercomparison of oxygenated volatile organic compound measurements at the SAPHIR atmosphere simulation chamber. *J. Geophys. Res. Atmos.* **2008**, *113*, D20307.
(38) Fuchs, H.; Holland, F.; Hofzumahaus, A. Measurement of tropospheric RO_2 and HO_2 radicals by a laser-induced fluorescence instrument. *Rev. Sci. Instrum.* **2008**, *79*, 084104.
(39) Holland, F.; Hofzumahaus, A.; Schäfer, J.; Kraus, A.; Pätz, H.-W. Measurements of OH and HO_2 radical concentrations and photolysis frequencies during BERLIOZ. *J. Geophys. Res. Atmos.* **2003**, *108*, 2−23.
(40) Holland, F.; Hessling, M.; Hofzumahaus, A. In Situ Measurement of Tropospheric OH Radicals by Laser-Induced Fluorescence—A Description of the KFA Instrument. *J. Atmos. Sci.* **1995**, *52*, 3393−3401.
(41) Fuchs, H.; Dorn, H.-P.; Bachner, M.; Bohn, B.; Brauers, T.; Gomm, S.; Hofzumahaus, A.; Holland, F.; Nehr, S.; Rohrer, F.; Tillmann, R.; Wahner, A. Comparison of OH concentration measurements by DOAS and LIF during SAPHIR chamber experiments at high OH reactivity and low NO concentration. *Atmos. Meas. Technol.* **2012**, *5*, 1611−1626.
(42) Cho, C.; Hofzumahaus, A.; Fuchs, H.; Dorn, H.-P.; Glowania, M.; Holland, F.; Rohrer, F.; Vardhan, V.; Kiendler-Scharr, A.; Wahner, A.; Novelli, A. Characterization of a chemical modulation reactor (CMR) for the measurement of atmospheric concentrations of hydroxyl radicals with a laser-induced fluorescence instrument. *Atmos. Meas. Technol.* **2021**, *14*, 1851−1877.
(43) Glowania, M.; Rohrer, F.; Dorn, H.-P.; Hofzumahaus, A.; Holland, F.; Kiendler-Scharr, A.; Wahner, A.; Fuchs, H. Comparison of formaldehyde measurements by Hantzsch, CRDS and DOAS in the SAPHIR chamber. *Atmos. Meas. Technol.* **2021**, *14*, 4239−4253.
(44) Lou, S.; et al. Atmospheric OH reactivities in the Pearl River Delta − China in summer 2006: measurement and model results. *Atmos. Chem. Phys.* **2010**, *10*, 11243−11260.
(45) Fuchs, H.; et al. Comparison of OH reactivity measurements in the atmospheric simulation chamber SAPHIR. *Atmos. Meas. Technol.* **2017**, *10*, 4023−4053.
(46) Jordan, A.; Haidacher, S.; Hanel, G.; Hartungen, E.; Märk, L.; Seehauser, H.; Schottkowsky, R.; Sulzer, P.; Märk, T. D. A high resolution and high sensitivity proton-transfer-reaction time-of-flight mass spectrometer (PTR-TOF-MS). *Int. J. Mass Spectrom.* **2009**, *286*, 122−128.
(47) Lindinger, W.; Hansel, A.; Jordan, A. On-line monitoring of volatile organic compounds at pptv levels by means of proton-transfer-reaction mass spectrometry (PTR-MS) medical applications, food control and environmental research. *Int. J. Mass Spectrom. Ion Processes* **1998**, *173*, 191−241.
(48) Wegener, R.; Brauers, T.; Koppmann, R.; Rodríguez Bares, S.; Rohrer, F.; Tillmann, R.; Wahner, A.; Hansel, A.; Wisthaler, A. Simulation chamber investigation of the reactions of ozone with short-chained alkenes. *J. Geophys. Res. Atmos.* **2007**, *112*, 2006JD007531.
(49) Bohn, B.; Rohrer, F.; Brauers, T.; Wahner, A. Actinometric measurements of NO_2 photolysis frequencies in the atmosphere simulation chamber SAPHIR. *Atmos. Chem. Phys.* **2005**, *5*, 493−503.
(50) Bohn, B.; Zilken, H. Model-aided radiometric determination of photolysis frequencies in a sunlit atmosphere simulation chamber. *Atmos. Chem. Phys.* **2005**, *5*, 191−206.
(51) Kaminski, M.; et al. Investigation of the beta-pinene photooxidation by OH in the atmosphere simulation chamber SAPHIR. *Atmos. Chem. Phys.* **2017**, *17*, 6631−6650.
(52) Jenkin, M. E.; Valorso, R.; Aumont, B.; Rickard, A. R. Estimation of rate coefficients and branching ratios for reactions of organic peroxy radicals for use in automated mechanism construction. *Atmos. Chem. Phys.* **2019**, *19*, 7691−7717.
(53) Novelli, A.; Cho, C.; Fuchs, H.; Hofzumahaus, A.; Rohrer, F.; Tillmann, R.; Kiendler-Scharr, A.; Wahner, A.; Vereecken, L. Experimental and theoretical study on the impact of a nitrate group on the chemistry of alkoxy radicals. *Phys. Chem. Chem. Phys.* **2021**, *23*, 5474−5495.
(54) Vereecken, L.; Nozière, B. H. migration in peroxy radicals under atmospheric conditions. *Atmos. Chem. Phys.* **2020**, *20*, 7429−7458.
(55) Atkinson, R.; Arey, J. Atmospheric Degradation of Volatile Organic Compounds. *Chem. Rev.* **2003**, *103*, 4605−4638.
(56) Färber, M.; Vereecken, L.; Fuchs, H.; Gkatzelis, G. I.; Rohrer, F.; Wedel, S.; Wahner, A.; Novelli, A. Impact of temperature-dependent non-PAN peroxynitrate formation, RO_2NO_2, on nighttime atmospheric chemistry. *Phys. Chem. Chem. Phys.* **2024**, *26*, 5183−5194.
(57) Finlayson-Pitts, B. J.; Pitts, J. N. J. *Chemistry of the Upper and Lower Atmosphere: Theory, Experiments and Applications*; Academic Press: San Diego, CA, 2000.
(58) Peeters, J.; Fantechi, G.; Vereecken, L. A Generalized Structure-Activity Relationship for the Decomposition of (Substituted) Alkoxy Radicals. *J. Atmos. Chem.* **2004**, *48*, 59−80.
(59) Orlando, J. J.; Tyndall, G. S.; Wallington, T. J. The Atmospheric Chemistry of Alkoxy Radicals. *Chem. Rev.* **2003**, *103*, 4657−4690.
(60) Martinez, M.; et al. OH and HO_2 concentrations, sources, and loss rates during the Southern Oxidants Study in Nashville, Tennessee, summer 1999. *J. Geophys. Res.* **2003**, *108*, 4617.
(61) Brune, W. H.; Baier, B. C.; Thomas, J.; Ren, X.; Cohen, R. C.; Pusede, S. E.; Browne, E. C.; Goldstein, A. H.; Gentner, D. R.; Keutsch, F. N.; Thornton, J. A.; Harrold, S.; Lopez-Hilfiker, F. D.; Wennberg, P. O. Ozone production chemistry in the presence of urban plumes. *Faraday Discuss.* **2016**, *189*, 169−189.
(62) Ren, X.; et al. Atmospheric oxidation chemistry and ozone production: Results from SHARP 2009 in Houston, Texas. *J. Geophys. Res. Atmos.* **2013**, *118*, 5770−5780.
(63) Atkinson, R.; Baulch, D. L.; Cox, R. A.; Crowley, J. N.; Hampson, R. F.; Hynes, R. G.; Jenkin, M. E.; Rossi, M. J.; Troe, J. Evaluated kinetic and photochemical data for atmospheric chemistry: Volume I - gas phase reactions of O_x, HO_x, NO_x and SO_x species. *Atmos. Chem. Phys.* **2004**, *4*, 1461−1738.
(64) Adachi, H.; Basco, N. Reactions of isopropylperoxy radicals with NO and NO_2. *Int. J. Chem. Kinet.* **1982**, *14*, 1243−1251.
(65) Peeters, J.; Vertommen, J.; Langhans, I. Rate Constants of the Reactions of CF_3O_2, i-$C_3H_7O_2$ and t-$C_4H_9O_2$ with NO. *Ber. Bunsenges. Phys. Chem.* **1992**, *96*, 431−436.
(66) Eberhard, J.; Villalta, P. W.; Howard, C. J. Reaction of Isopropyl Peroxy Radicals with NO over the Temperature Range 201-401 K. *J. Phys. Chem.* **1996**, *100*, 993−997.
(67) Atkinson, R.; Baulch, D. L.; Cox, R. A.; Crowley, J. N.; Hampson, R. F.; Hynes, R. G.; Jenkin, M. E.; Rossi, M. J.; Troe, J. Evaluated kinetic and photochemical data for atmospheric chemistry: Volume II - gas phase reactions of organic species. *Atmos. Chem. Phys.* **2006**, *6*, 3625−4055.
(68) Atkinson, R. Rate constants for the atmospheric reactions of alkoxy radicals: An updated estimation method. *Atmos. Environ.* **2007**, *41*, 8468−8485.
(69) Gkatzelis, G. I.; Coggon, M. M.; McDonald, B. C.; Peischl, J.; Gilman, J. B.; Aikin, K. C.; Robinson, M. A.; Canonaco, F.; Prevot, A. S. H.; Trainer, M.; Warneke, C. Observations Confirm that Volatile

https://doi.org/10.1021/acsestair.4c00064
ACS EST Air 2024, 1, 1096−1111

Chemical Products Are a Major Source of Petrochemical Emissions in U.S. Cities. *Environ. Sci. Technol.* **2021**, *55*, 4332−4343.
(70) Asif, Z.; Chen, Z.; Haghighat, F.; Nasiri, F.; Dong, J. Estimation of Anthropogenic VOCs Emission Based on Volatile Chemical Products: A Canadian Perspective. *Environ. Manage.* **2023**, *71*, 685−703.
(71) Coggon, M. M.; McDonald, B. C.; Vlasenko, A.; Veres, P. R.; Bernard, F.; Koss, A. R.; Yuan, B.; Gilman, J. B.; Peischl, J.; Aikin, K. C.; DuRant, J.; Warneke, C.; Li, S.-M.; De Gouw, J. A. Diurnal Variability and Emission Pattern of Decamethylcyclopentasiloxane (D_5) from the Application of Personal Care Products in Two North American Cities. *Environ. Sci. Technol.* **2018**, *52*, 5610−5618.
(72) Färber, M.; Fuchs, H.; Bohn, B.; Carlsson, P. T. M.; Rohrer, F.; Novelli, A. Atmospheric simulation chamber study: propane + OH - Gas-phase oxidation - product study - 2022-05-13. *AERIS [DATA SET]*, 2024, *Version 1.0*. DOI: 10.25326/PVYS-HR72.
(73) Färber, M.; Fuchs, H.; Bohn, B.; Carlsson, P. T. M.; Rohrer, F.; Novelli, A. Atmospheric simulation chamber study: propane + OH - Gas-phase oxidation - product study - 2022-06-07. *AERIS [DATA SET]*, 2024, *Version 1.0*. DOI: 10.25326/A5ZM-W179.
(74) Färber, M.; Fuchs, H.; Bohn, B.; Carlsson, P. T. M.; Rohrer, F.; Novelli, A. Atmospheric simulation chamber study: propane + OH - Gas-phase oxidation - product study - 2022-05-18. *AERIS [DATA SET]*, 2024, *Version 1.0*. DOI: 10.25326/A742-9J73.
(75) Färber, M.; Fuchs, H.; Bohn, B.; Gkatzelis, G. I.; Rohrer, F.; Wedel, S.; Novelli, A. Atmospheric simulation chamber study: propene + OH - Gas-phase oxidation - product study - 2022-06-09. *AERIS [DATA SET]*, 2024, *Version 1.0*. DOI: 10.25326/B0ZW-YQ76.
(76) Färber, M.; Fuchs, H.; Bohn, B.; Carlsson, P. T. M.; Gkatzelis, G. I.; Rohrer, F.; Wedel, S.; Novelli, A. Atmospheric simulation chamber study: propene + OH - Gas-phase oxidation - product study - 2022-06-23. *AERIS [DATA SET]*, 2024, *Version 1.0*. DOI: 10.25326/0T20-XY65.
(77) Färber, M.; Fuchs, H.; Bohn, B.; Gkatzelis, G. I.; Rohrer, F.; Wedel, S.; Novelli, A. Atmospheric simulation chamber study: *trans*-2-hexene + OH - Gas-phase oxidation - product study - 2022-05-24. *AERIS [DATA SET]*, 2024. DOI: 10.25326/P6Q8-0N05.
(78) Färber, M.; Fuchs, H.; Bohn, B.; Gkatzelis, G. I.; Marcillo Lara, A. C.; Rohrer, F.; Wedel, S.; Novelli, A. Atmospheric simulation chamber study: isopentane + OH - Gas-phase oxidation - product study - 2022-06-21. *AERIS [DATA SET]*, 2024, *Version 1.0*. DOI: 10.25326/ZQHP-BA18.
(79) Färber, M.; Fuchs, H.; Bohn, B.; Gkatzelis, G. I.; Marcillo Lara, A. C.; Rohrer, F.; Wedel, S.; Novelli, A. Atmospheric simulation chamber study: isopentane + OH - Gas-phase oxidation - product study - 2022-06-11. *AERIS [DATA SET]*, 2024, *Version 1.0*. DOI: 10.25326/A5RG-3327.
(80) Färber, M.; Fuchs, H.; Bohn, B.; Gkatzelis, G. I.; Marcillo Lara, A. C.; Rohrer, F.; Wedel, S.; Novelli, A. Atmospheric simulation chamber study: isopentane + OH - Gas-phase oxidation - product study - 2022-06-16. *AERIS [DATA SET]*, 2024, *Version 1.0*. DOI: 10.25326/87E2-JF37.
(81) Färber, M.; Fuchs, H.; Bohn, B.; Carlsson, P. T. M.; Gkatzelis, G. I.; Marcillo Lara, A. C.; Rohrer, F.; Wedel, S.; Novelli, A. Atmospheric simulation chamber study: n-hexane + OH - Gas-phase oxidation - product study - 2022-05-19. *AERIS [DATA SET]*, 2024, *Version 1.0*. DOI: 10.25326/QJYB-JW72.
(82) Färber, M.; Fuchs, H.; Bohn, B.; Carlsson, P. T. M.; Gkatzelis, G. I.; Marcillo Lara, A. C.; Rohrer, F.; Wedel, S.; Novelli, A. Atmospheric simulation chamber study: n-hexane + OH - Gas-phase oxidation - product study - 2022-05-22. *AERIS [DATA SET]*, 2024, *Version 1.0*. DOI: 10.25326/2GGT-JY88.
(83) Vereecken, L. *Replication Data for: Effect of the alkoxy radical chemistry on the ozone formation from anthropogenic organic compounds investigated in chamber experiments*. 2024. DOI: 10.26165/JUELICH-DATA/J2LHTQ.

https://doi.org/10.1021/acsestair.4c00064
ACS EST Air 2024, 1, 1096−1111